processes

MDPI

Article

Isosteric Heat: Comparative Study between Clausius–Clapeyron, CSK and Adsorption Calorimetry Methods

Liliana Giraldo [1], Paola Rodriguez-Estupiñán [2] and Juan Carlos Moreno-Piraján [2,*]

[1] Departamento de Química, Universidad Nacional de Colombia, Bogotá 11001, Colombia; lgiraldogu@unal.edu.co

[2] Departamento de Química, Facultad de Ciencias, Universidad de los Andes, Bogotá 111711, Colombia; jp.rodrigueze@uniandes.edu.co

* Correspondence: jumoreno@uniandes.edu.co; Tel.: +57-1-3394949 (ext. 2786)

Received: 8 March 2019; Accepted: 4 April 2019; Published: 10 April 2019

Abstract: This work presents the calorimetric study of five adsorbents with different chemical and textural characteristics: MOF-199, MCM-41, SBA-15, activated carbon prepared from corn cob (GACKP) and graphite. These solids were used to establish the differences between isosteric heats evaluated by three different methods: Clausius–Clapeyron (C-C), Chakraborty, Saha and Koyama (CSK) and Adsorption Calorimetry (A-Cal). The textural characterization results show solids that have values of specific surface area between 2271 $m^2 \cdot g^{-1}$ for the MOF-199 and 5.2 $m^2 \cdot g^{-1}$ for the graphite. According to the results obtained for the isosteric heats for each sample, the magnitude varies depending on the coverage of the adsorbate and the textural characteristics of each adsorbent. Solids with an organized structure have isosteric heat values that are coincident among the three methods. Meanwhile, heterogeneous solids such as activated carbon values evaluated by the CKS and C-C have a high dispersion method regarding the adsorption calorimetry method. The results obtained show that the adsorption calorimetry, being a direct experimental measurement method, presents less dispersed data. At low quantities, the isosteric heat of nitrogen adsorption decreased in the order MOF-199, GACKP, MCM-41, SBA-15 and Graphite. The order for the isosteric heats values was coherent with the surface characteristics of each of the solids, especially with the pore size distribution. Finally, throughout the coverage examined in this work, the isosteric heats for nitrogen adsorption determined by adsorption calorimetry (A-Cal) were larger than the evaluated by C-C and CSK indirect methods of vaporization. According to the results, it is shown that the adsorption calorimetry allows values of the isosteric heats of adsorption with an error of less than 2% to be established and also reveals the complex nature of the heterogeneity or homogeneity of the adsorbent.

Keywords: isosteric heats; adsorption calorimetry; CKS isosteric; Clausius–Clapeyron

1. Introduction

A fundamental aspect of the thermodynamic study of surface processes is the determination of adsorption heat with good precision [1]. This variable is directly related to adsorbate–adsorbent interactions and the behavior of porous materials in applications such as gas storage and separation [2–5] and in technology for separation and purification of gas mixtures like Pressure swing adsorption (PSA) [5–7]. It has been established that the determinations of the heat effects associated with the adsorbate–adsorbent interactions are usually more sensitive to the adsorption isotherms [5,7] and for this reason some authors have proposed that carrying out a combination of heat

measurements and adsorption capacity will provide complementary information to understand gas adsorption processes [5]. Experimentally, two methods are used to evaluate the heat of adsorption [5,8]. The first one is the calorimetric method (usually called direct method), which directly evaluates the heat released when the adsorbate is in contact with the adsorbent and the other method is the isosteric (indirect method) in which a quantitative relationship between pressure and temperature is measured at a constant amount of the adsorbed substance and the adsorbent [5].

Isosteric measurements are usually used more than calorimetric measurements. Different reasons have been presented by the authors: some proposed that direct determination of heat effects is often complicated and more costly, particularly in non-environmental conditions [5]. While it is assumed that the approaches of direct and indirect methods should give identical results, often ambiguity is generated, mainly due to the definitions of the isotherms and the choice of different thermodynamic models to adjust the corresponding adsorption isotherms [5,8–11]. The experimental results of the isosteric heat are very sensitive to the conditions of the adsorption isotherms, particularly if the analysis of the data is available only for a limited number of temperatures [5]. Isosteric analysis often leads to inconsistencies or even erroneous conclusions under conditions that are not ideal [2,4] because the thermodynamic analysis is based on the numerical adjustment of the adsorption isotherms using semi-empirical models, such as Langmuir single-site or dual-site models [5,12,13], the Toth model [14–16] or the virial equation [17–20]. Although semi-empirical parameters can be correlated with a binding affinity between adsorbate and adsorbent [20], they are significant only in the context of specific isotherms [5].

As mentioned by Tian et al. [5,6,21–26], the correct determination of isosteric heat is fundamentally associated with defining the adsorbed phase. It was J. W. Gibbs who introduced this concept for heterogeneous systems in one of his first works in thermodynamics. From the point of view of the definitions of Gibbs to describe the properties of a surface and the interface, the latter can be represented as a two-dimensional dividing surface without any volume [5,21–30]; isosteric heat is often interpreted as the energy to transfer an adsorbate molecule from the bulk of the fluid phase to the adsorbed phase under some fixed thermodynamic conditions of the system such as temperature, total volume and amount of adsorbent [26–31]. Some authors have analyzed that the Gibbsian formalism predicts non-physical isosteric heat under maximum thermodynamic conditions of the adsorption isotherm. However, unlike bulk systems, the properties of the adsorbed phase cannot be defined only with the excess surface area for each component [23–26,28]. Gibbs thermodynamics predict a non-physical isosteric heat when the adsorption isotherm exhibits a maximum [5,28–37].

In summary, the isosteric heat of adsorption allows characterization of the surface properties of adsorbents, catalysts and other materials [1], provides information on the homogeneity and heterogeneity of materials, for example allows study of the degree of graphitization of carbons [2–6], the formation of liquid films [7], the formation of molecular multilayers on a surface and the evaluation the adsorption energy distribution (AED) [8,36,38].

The isosteric heats of adsorption for a specific adsorbate can be calculated by applying the Clausius–Clapeyron (C-C) equation on the isothermal data at two different temperatures the formal derivation of the C-C equation can be found in the work of Pan et al. [39]. However, the simplification of the heterogeneity in the adsorbate–adsorbent interaction and the modeling isotherms for analyzing the experimental data, fail to completely explain the ΔH_{ads} across all the range of pressures [23,24].

Some authors in recent works [22,24–26] have developed very rigorous thermodynamic studies to deduce isosteric heat without inconsistencies and that can be used for practical applications [21,31,38]. Among other very interesting methods that have also been applied to assess isosteric heat, the outstanding work of Chakraborty et al. [23–26] should be mentioned, who developed a theory to determine the isosteric heat of adsorption between an adsorbate (vapor) and an adsorbent (solid) based on the thermodynamics of chemical equilibrium, Maxwell's relations and the entropy of the adsorbed phase. They presented an equation to calculate the isosteric heat of adsorption by making an adjustment to the Clausius–Clapeyron equation.

The Chakraborty, Saha and Koyama model (this model will be identified in this work with the acronym "CSK") obtains the expression of ΔH_{ads} from the concepts of chemical equilibrium potentials between the gaseous and adsorbed phases and the state equation, as well as the Maxwell relationships. Using these relationships and the chemical potential gradient of P and T with respect to entropy and specific volumes, respectively. The CSK model derives the expression ΔH_{ads} to calculate the isosteric heat.

On the other hand, the adsorption calorimetric measurements (A-Cal) provide reliable information related to surface chemical composition, and energetic parameters related to adsorbate–adsorbent interactions in the micropore region.

In this work, the isosteric heat of adsorption is evaluated for porous solids that have different textural and chemical characteristics, using three methods reported in the literature. The methods used are: the method developed by Chakraborty et al. (CSK) [24–26], the Clausius–Clapeyron method (here it will be identified as: C-C) and finally by the direct method by adsorption calorimetry using the N_2 molecule as adsorbate. In this way, it is proposed to compare the results obtained for isosteric heat using the methods of CSK and C-C (indirect methods) with the method calculated direct by adsorption calorimetry (A-Cal), and provides an experimental tool that allows evaluation of characteristics of the samples as well as establish some advantages of using each of the above mentioned methods.

2. Materials and Methods

2.1. Porous Solids

2.1.1. Synthesis of MOF-199

MOF-199 was prepared by a modification of the synthesis procedure described in the literature followed very closely [40–43]. In a typical preparation [44], a solid mixture of Cu $(NO_3)_2 \cdot 3H_2O$ (0.654 g, 2.22 mmol, Merck®, Kenilworth, NJ, USA) and 1,3,5-benzenetricarboxylic acid (H_3BTC) (0.326 g, 1.55 1mmol, Merck®, Kenilworth, NJ, USA) was dissolved in a mixture of DMF (3 mL Merck®, Kenilworth, NJ, USA), ethanol (4 mL, Merck®, Kenilworth, NJ, USA) and water (2 mL) in a 20 mL vial. The vial was heated at 85 °C in an isothermal oven for 48 h, yielding light blue crystals. After cooling the vial to room temperature, the solid product was obtained by decanting with mother liquor and washed with DMF (4 × 9 mL). Solvent exchange was then carried out with ethanol (4 × 9 mL) at room temperature. The product was then dried under vacuum (at ≤5 mTorr overnight) at 170 °C for 8 h, yielding 0.345 g of MOF-199 during which time, the deep blue solid became blue-violet [42].

2.1.2. Synthesis of Mesostructured Silica, MCM-41

MCM-41 was prepared according to Melendez et al. methodology [45], with some small changes in terms of amounts used in the laboratory. The procedure was as follows: Solution A, a desired amount of CTAB (Cetyl Trimethyl Ammonium Bromide) was mixed with 8.5 mL of 4.5-propanol (Merck®, Kenilworth, NJ, USA) and 100 mL of deionized water. Solution B, 4.6 g of Na_2SiO_3 solution (Merck®, Kenilworth, NJ, USA) was dissolved in 45 mL of deionized water and then both solutions A and B was cooled at 2 °C. Then, the solution B was slowly added dropwise to solution A under constant stirring for 4 h, then 25 mL of ethyl acetate (Merck®, Kenilworth, NJ, USA) was added, and the solution was stirred for 2.5 h. The mixture was carried to a temperature of 40 °C, under constant stirring. At the end of this time, the reaction temperature was increased to 85 °C for a period of 72 h in static conditions. The precipitate obtained was collected by filtration and washed with deionized water. Finally, the solid was calcined for 12 h at 550 °C.

2.1.3. Synthesis of SBA-15

Another of the materials that was used in this research to compare the results of isosteric heats using the three different methods were the nanoparticles based on silica produced at the University of California, Santa Barbara, CA, USA, so this material has the initials in the name: SBA-15. These particles

have a hexagonal organization of their pores. These SBA-15 mesoporous silica nanoparticles were prepared based on reports from the scientific literature making some small changes [46–48]. In the synthesis carried out in this work, we used Pluronic P123 triblock as mold in acidic conditions. The procedure used was to dissolve 12.75 g of Pluronic P123 in 500 mL of 2.5 M hydrochloric acid (Merck®, Kenilworth, NJ, USA) under constant stirring conditions (approximately 450 rpm) at a temperature of 40 °C. The silica precursor, TEOS (Tetraethyl orthosilicate), was then added to this micellar solution and the mixture was continuously stirred at the same regime for 48 h at the same temperature of reaction. The reaction was carried out in a reactor manufactured especially for this synthesis and made in Teflon. During this phase of the synthesis, the particles that were generated were modified and their shape changed due to the addition of the silica precursor, resulting in a more orderly material. Then, the temperature rose to 100 °C to carry out what is called the hydrothermal process that was carried out for 72 h. During this hydrothermal treatment, the hydrophilic portions of Pluronic 123 became less soluble in water and, therefore, retracted into the hydrophobic core of the micelle. Finally, the material was recovered by filtration in the presence of toluene and ethanol after continuous stirring and the sample was then dried in an oven at 90 °C for 24 h. Finally, the sample was calcined in an oven at 550 °C for 5 h. The parts of the product must be collected before calcination for characterization.

2.1.4. Preparation of Activated Carbons from Corn Cobs

The corn cob (CC) used for the preparation of activated carbons was collected in a market in Bogotá (Cundinamarca, Colombia). The CC impurities were eliminated by means of a thorough washing with distilled water, initially at room temperature and then with water at 50 °C. In this way, the impurities that this material bring were eliminated. Next, the corn cobs were placed in an oven at a temperature of 105 °C, for a period of 48 h to remove the moisture content. In order to give a homogeneous size to the particles with which it is going to work, the material was subjected to a grind to achieve a size of 0.3 to 0.5 cm. To prepare the activated carbon samples, the cob samples were carbonized under the following conditions: at 450 °C with a heating rate of 5 °C min^{-1} for 1.5 h under inert atmosphere. The material was previously treated with a solution of H_3PO_4 (Merck®, Kenilworth, NJ, USA); the impregnation ratio (H_3PO_4/char) was equal to 1, the mixture was placed in an oven at 80 °C for 24 h, to ensure adequate impregnation between the adsorbent and the activating agent. Subsequently, the resulting solid was washed in batches with portions of hot distilled water until reaching a stable pH value close to neutrality. Then, the activation of the material was carried out, impregnation was carried out with KOH solution (Merck®, Kenilworth, NJ, USA) in a ratio of 6:1 and the material was taken at a temperature of 780 °C for 1 h in a nitrogen atmosphere with a heating rate of 5 °C min^{-1}. Then, the oven was allowed to cool to room temperature. The activated carbon obtained in this way was washed with double deionized water, several times, and then washed with hydrochloric acid and water (100 mL of HCl, Merck®, Kenilworth, NJ, USA and 300 mL of double-deionized water) to remove the excess residues of activating agent and inorganic matter from the sample. Finally, a careful final wash was carried out with double deionized water until a constant pH was reached [48,49]. This sample obtained through this procedure, in this work was labeled as GACKP.

2.1.5. Graphite

In this research, Aldrich™ brand graphite (Darmstadt, Germany) was used. According to company specifications, graphite has a purity of ≥98% in carbon, ≤300 (mesh).

2.2. Measurement and Characterization

2.2.1. Nitrogen Adsorption-Desorption Isotherms at −196 °C

Nitrogen adsorption-desorption isotherms were obtained at −196 °C using a sortometer automatic apparatus IQ_2, Quantachrome, Miami, FL, USA. The samples were degassed for 6 h under vacuum at 200 °C prior to any adsorption experiment.

2.2.2. Thermogravimetric Analysis (TGA)

Differential thermal analysis (DTA) and thermal gravimetric (TG) were performed on a STA7000 Series Simultaneous Thermal Analyzer (STA) instrument, Hitachi™, (Tokyo, Japan). Approximately 10–20 mg of adsorbent was placed in a platinum crucible on the pan of a microbalance and then heated from room temperature up to 800 °C at a heating rate of 2 °Cmin^{-1} while being purged with argon at a flow rate of 100 mLmin^{-1} and constantly weighed.

2.2.3. Infrared Spectroscopy (FTIR) and XRD of Samples used in this Research

Fourier transform infrared spectroscopy (FTIR) absorbance spectra of adsorbents synthesized were obtained through the KBr technique, with the analysis performed on a Nicolet™ iS™50 FT-IR spectrometer (Madison, WI, USA) in the wave number range of 400–4000 cm^{-1}.

On the other hand, Powder X-ray diffraction (XRD) (PXRD) patterns were recorded on an X-ray diffractometer (MiniFlex II, Rigaku, Japan) at 30 kV and 15 mA using Cu Kα (λ = 1.5418 Å) radiation, with a scanning speed of 4° min^{-1}, a step size of 0.01° in 2 h, and scanning range of 3–40°.

2.2.4. SEM of Adsorbents

Analyses of the morphology, chemical composition and the elemental maps of the samples were conducted by JEOL JSM-7100FA field emission Scanning Electron Microscope equipped with an energy dispersive X-ray (EDX) system (Freising, Germany).

2.2.5. Differential Enthalpy Measurement by Adsorption Calorimetry

The differential enthalpy of nitrogen adsorption measurements was obtained in a high sensitivity Tian-Calvet heat flow microcalorimeter. This equipment was designed and built in Porous Solids and calorimetry laboratory (Author's Laboratory) [50,51]. Prior to each experiment, the samples were degassed at 250 °C and 1 × 10^{-6} MPa for 24 h. The microcalorimeter uses two calorimetric cells: the first one contains the sample, and the second one acts as a reference, it is usually empty. The experiments were conducted in an isothermal manner by gradually feeding increasing small doses of nitrogen over previously degassed samples. The initial dose sent to the system corresponded to a pressure of 10 mbar. Since the initial dose was sufficiently small, the heat obtained can be considered as a differential adsorption heat. A new dose of nitrogen (10 mbar) was then added until equilibrium pressure was achieved. Subsequently, the nitrogen dose was increased, and the procedure was repeated until no change in pressure was observed. This was achieved at around 35 bar (3.5 MPa). The adsorption pressures in the measurements were monitored with Baratron pressure transducers (Andover, MA, USA) to record low pressures and a Honeywell type Model HP High-Pressure Transducer (MKS Instrument, Andover, MA, USA) to record the changes at high pressures. The calorimeter allows sensing the heat generated by each dose added and the pressure drop in the cell allows obtaining the amount adsorbed. The calorimetric adsorption experiments finished when the released heat at a relatively high pressure and the increase in adsorbed amount were insignificant [52–55]. The calorimeter was calibrated electrically in order to establish its correct operation as well as to convert the voltage-time signal into units of energy. The constant established for this equipment was 25.4 ± 0.3 WV^{-1}.

2.2.6. Evaluation of Isosteric Heat of Adsorption by Clausius–Clapeyron (C-C)

The differential enthalpy of adsorption at constant coverage or what is known as the isosteric method can be evaluated by determining the isotherms in the lab at two or more different temperatures. Taking these isotherms as a starting point, it is possible to perform the respective data processing and relate them by means of a graphical representation the pressure logarithm, ln p, for a given amount adsorbed n_a as a function of the reciprocal temperature, 1/T. Then, using the Clausius–Clapeyron equation it is possible to establish the isometric heat of adsorption. It is usually assumed that there is no enthalpy or entropy variation with temperature. The thermodynamic expression used is:

$$\Delta_{ads}\dot{h}_{n_a} = R\left(\frac{\partial \ln[P]}{\partial \frac{1}{T}}\right)_{n_a}, \quad (1)$$

where $\Delta_{ads}\dot{h}_{n_a}$ is the enthalpy of differential adsorption and R is the gas constant. Some authors affirm that it is possible to measure two isotherms with 10 K difference, i.e., for liquid nitrogen (77 K) and liquid argon (87 K); therefore, it is possible to relate the equilibrium pressures P_1 and P_2 to the corresponding temperatures T_1 and T_2 for a given amount adsorbed:

$$\Delta_{ads}\dot{h} = \frac{RT_1T_2}{T_2 - T_1}\ln\frac{P_2}{P_1}. \quad (2)$$

According to this, it is noteworthy that the accuracy of this type of calculation depends on the measurement of the pressure and eventually problems arise at low pressures. This is mainly due to the accuracy of the adsorbent-adsorbent balance and not to the pressure reading accuracy, because the pressure gauges are usually more than sufficient, especially in the case of the adsorbate load in the range of the micropores in materials that are poorly conductive, as in the case of silica: some authors have shown that a small deviation in equilibrium due to molecular diffusion or thermal transfer can generate a relatively large variation in pressure measurements [56]. This argument can in some cases explain the dispersion in the results obtained using the isosteric method.

2.2.7. Evaluation of the Isosteric Heats of Adsorption by Chakraborty-Saha-Koyama (CSK)

The CSK model [24–26] proposes the calculation of the isosteric heat of adsorption using a series of thermodynamic arguments that allows obtaining an expression to evaluate this parameter (ΔH_{ads}). The development of this model can be found in Chakraborty et al. [24]. The fundamental expression taken from [24] is shown to contextualize the reader about the equation that was used to deduce the isosteric heat in this work. The CSK model obtains the expression of ΔH_{ads} from the concepts of chemical equilibrium potentials between the gaseous and adsorbed phases and the state equation, as well as the Maxwell relationships, using these relationships and the chemical potential gradient of P and T with respect to entropy and specific volumes, respectively. The CSK model derives the expression ΔH_{ads} to calculate the isosteric heat. Following the development of CSK, the following expression is obtained [24]:

$$\Delta_{ads} \cong TV_g\left(\frac{\partial P}{\partial m_a}\right)_T\frac{dm_a}{dT} + RT^2\left[\left(\frac{\partial(\ln P)}{\partial T}\right)_{m_a}\right] = TV_g\left(\frac{\partial P}{\partial m_a}\right)_T\frac{dm_a}{dT} + \Delta H_{ads}. \quad (3)$$

V_g: Specific volume of the gas
T: Temperature
P: Pressure
m_a: Adsorbate mass
ΔH_{ads}: Conventional form of Clausius–Clapeyron isosteric heat (C-C)

3. Results and Discussion

3.1. Porous Texture Analysis

Table 1 shows the textural parameters determined by the N_2 adsorption isotherms at −196 °C: apparent surface area, S_{BET}, by the Brunauer–Emmett–Teller (BET) method [32]; (ii) Dubinin−Radushkevich (DR) micropore volume, V_{DR}, [57,58]. Therein; (iii) total pore volume, $V_{0.99}$, defined as the volume of liquid nitrogen corresponding to the amount adsorbed at a relative pressure $P/P^{\circ} = 0.99$ [39,57,58]. The mesopores volume, V_{me}, was calculated as the difference $V_{0.99} - V_{DR}$. The average micropore diameter, L_0, and adsorption energy, E_o, were also calculated [57–59], as well as the pore size distributions (PSD) by application of the Density Functional Theory (DFT) [39,56–59]. The samples have a wide range of textural properties, such as the apparent surface area ranging from 5.2 m^2g^{-1} for graphite to 2271 m^2g^{-1} for MOF-199. Most prepared samples are mainly microporous if one takes into account the ratio, $V_{DR}/V_{0.99}$, which varied from 0.83 to 094. The graphite does not have a porosity as expected.

Table 1. Textural parameters of all samples from the N_2 adsorption-desorption isotherm at −196 °C.

Samples	S_{BET} ($m^2 \cdot g^{-1}$)	$V_{0.99}$ ($cm^3 \cdot g^{-1}$)	V_{DR} ($cm^3 \cdot g^{-1}$)	Eo ($kJ \cdot mol^{-1}$)	Lo (nm)	$V_{DR}/V_{0.99}$	V_{Meso} ($cm^3 \cdot g^{-1}$)
MOF-199	2271	0.66	0.62	8.47	7.3	0.94	0.04
MCM-41	1274	0.44	0.40	3.58	8.4	0.91	0.04
SBA-15	663	0.24	0.17	5.41	6.2	0.83	0.07
GACKP	856	0.33	0.28	9.32	7.1	0.85	0.05
Graphite	5.2	0.10	-	7.25	0.3	-	0.001

Taking into account the scope of this work, the materials have a diversity in the textural properties which will allow analyzing the effect of these characteristics with respect to the evaluation of the isosteric heats using the three methods proposed in this investigation.

Figure 1a shows the N_2 adsorption-desorption isotherms at −196 °C for all the samples used in this study. The isotherm for the MCM-41 presents an isotherm type IV, characteristic of materials with a uniform cylindrical mesoporous system. It also presents a hysteresis loop of type H3, which corroborates the previous statement, because this type of hysteresis is characteristic of solid particles solid formed by cylindrical channels, aggregates (consolidated) or agglomerated (not consolidated) of spheroidal particles [60,61].

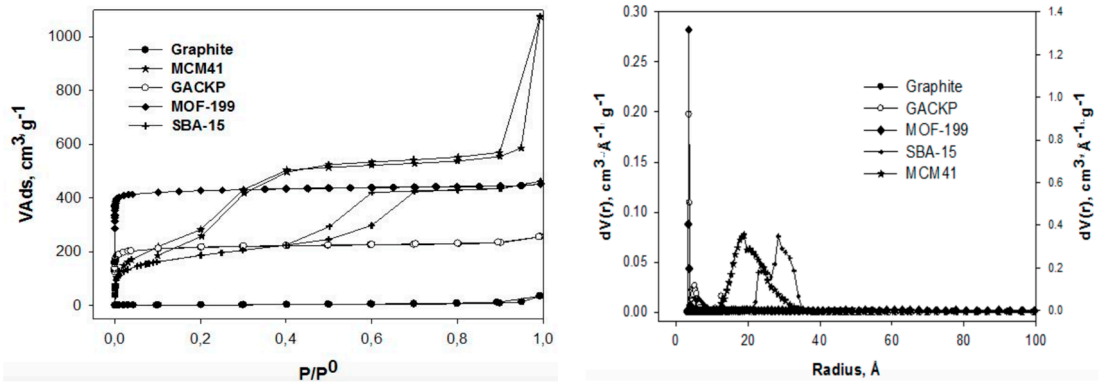

(**a**) (**b**)

Figure 1. N_2 adsorption-desorption isotherms (**a**) and (**b**) pore size distributions by DFT models.

It is interesting to note that the N_2 adsorption isotherm of the MCM-41 shows three different steps. The first step (P/P° = 0.0–0.2) corresponds to monolayer-multilayer adsorption on the walls of the pores. The second step (P/P° = 0.2–0.3), resembles typical adsorption of a well-defined capillary condensation within the mesopores [34]. A very sharp step (third step) occurs between 0.3 and 0.4 P/P° is due to the uniform filling pores of the hexagonal lattice. The H3 hysteresis loop was observed between 0.4 and 1.0 P/P°. This loop is associated with the multilayer adsorption on the outer surface of the crystals [44,61].

As for the N_2 adsorption isotherm corresponding to the SBA-15, it presents an isotherm type IV according to the IUPAC classification, which are typical for mesoporous solids and presents a hysteresis loop type H1, which indicates the existence of mesopores and in this particular case of the two-dimensional hexagonal distributions of the pores, which are very characteristic of mesoporous SBA-15 matrices [62,63]. The isotherm shows an elongated inflection in the P/P° range of 0.40 to 0.70 characteristic of capillary condensation within uniform pores.

The N_2 adsorption isotherm corresponding to MOF-199 is type I (a) according to the recent recommendations of the IUPAC [63]; this is a typical reversible isotherm with a high adsorption capacity at low relative pressures. Based on the N_2 isotherm, the Brunauer–Emmett–Teller surface area (BET) of the MOF-199 prepared for this investigation was 2271 $m^2 \cdot g^{-1}$, the highest area within the five samples to be studied in this work. This value is comparable for highly porous Metal-Organic Frameworks (MOF´s) reported in the scientific literature [64–67]. Meanwhile, the $V_{0.99}$ is 0.66 $cm^3 \cdot g^{-1}$, while the V_{DR} is slightly lower: 0.62 $cm^3 \cdot g^{-1}$, but very coherent between them.

Similar behavior was found for the isotherm of the activated carbon obtained from the corn cob, GACKP, whose isotherm is also type I with a completely reversible behavior and without the presence of a hysteresis loop. It presents high and rapid adsorption of N_2 at low pressures and then reaches a plateau after a P/P° of 0.1.

The isotherm for graphite is type V according to the IUPAC report [62]. In the low P/P^o range of nitrogen, this isotherm is very similar to type III and this can be attributed to relatively weak adsorbent–adsorbent interactions. At higher P/P°, the pore filling follows the molecular grouping. This behavior is classic for samples that do not have porosity. As reported in Table 1, it does not have pores.

The values of the characteristic energies of prepared solids are between 3.58 and 9.32 $kJ \cdot mol^{-1}$, it can be deduced according to the order of magnitude that prepared solids have a great potential for the adsorption of nitrogen molecules on their surfaces.

Figure 1b shows the PSD's calculated by Density Functional Theory (DFT) for samples prepared for this study. It can be seen that the samples MCM-41 and SBA-15 have radii of 18 and 35 Å respectively. The other samples have PSDs towards lower radius values.

Porosity size distribution was performed using the Non-Local Density Functional Theory (NLDFT) and Quenched Solid Density Functional Theory (QSDFT) models, applying slit, cylinder and combined pore geometry. The results obtained with the AsiQWin software of IQ2 Autosorb (Quantachrome Inc. Boynton Beach, FL, USA) are shown in Figure 2a–e. The samples, in general, were more adjusted to the NLDFT model. The DFT models that adjusted better for each one of the studied samples taking into account the geometry pore were: for GACKP, QSDFT cylinder-slit geometry, while NLDFT describe better the experimental data of graphite, with slit pore geometry, SBA-15, and MCM-41, with cylinder pore geometry, and MOF-199, with a combined geometry (cylinder-slit). The sample that has a better fit to the QSDFT model is characterized by having rough and energetically heterogeneous surfaces, characteristic of activated carbons obtained from lignocellulosic waste, while NLDFT describes a geometric and energetic homogeneous surface, just as expected from the mesostructured silicas and the graphene layers of the graphite.

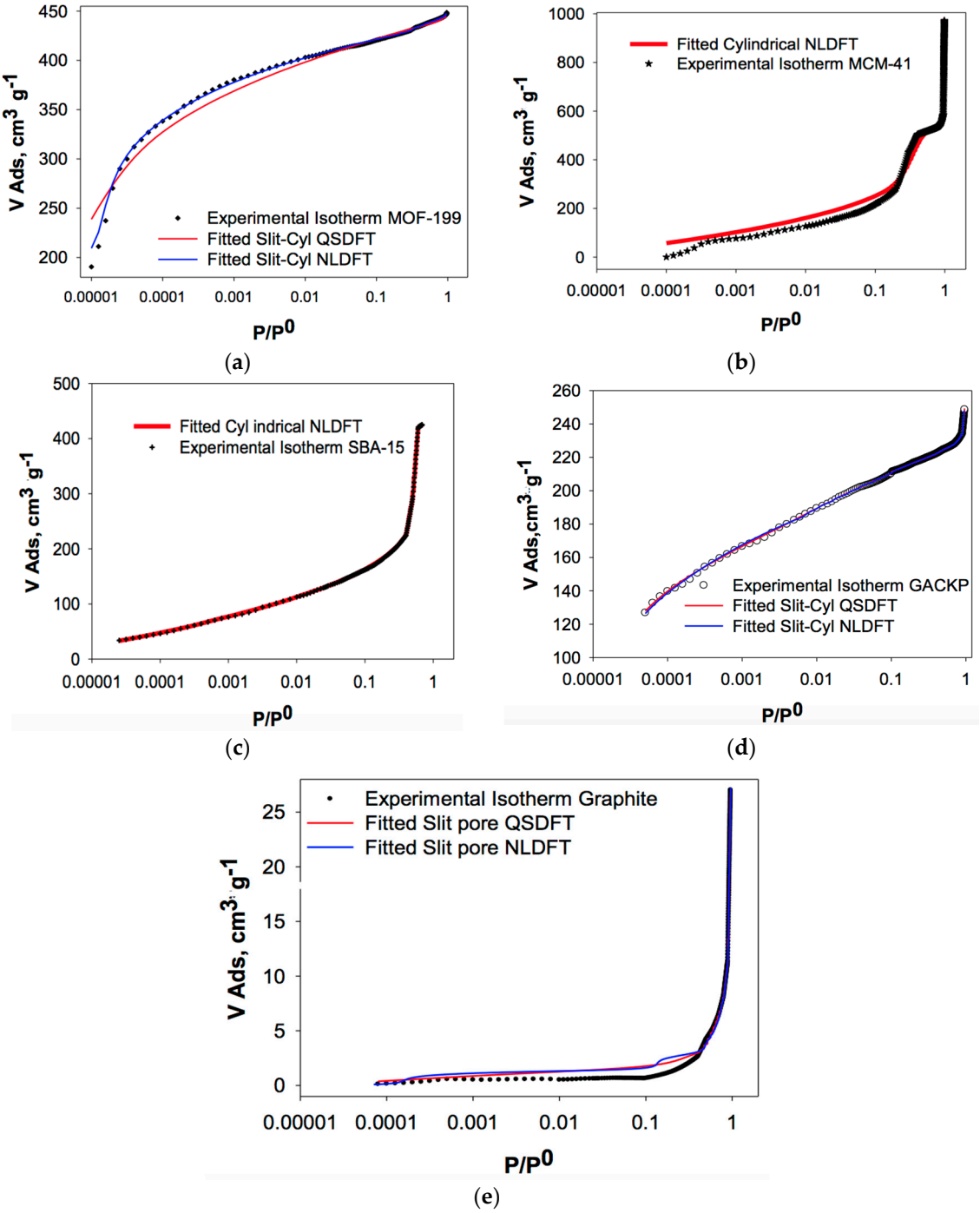

Figure 2. Comparison between QSDFT (Quenched Solid Density Functional Theory) and NLDFT (Non-Local Density Functional Theory) models for nitrogen adsorption of samples prepared in this work. Experimental isotherms and fitted models plotted in logarithmic (semi-scale) for (**a**) MOF-199, (**b**) MCM-41, (**c**) SBA-15, (**d**) GACKP and (**e**) Graphite.

Table 2 shows the % error fitting, a software calculated parameter (AsiQWin) that relates the adjustment between the experimental and modeled data according to pore geometry and the NLDFT and QSDFT models. DFT Pore Size Distributions (PSD) between 5 to 100 Å (Figure 1b) reflect the different nature in the porosity of the samples. The results are in good agreement with the textural analyses done so far in this investigation.

Table 2. Mean error adjustments between different surface textures (NLDFT vs. QSDFT) in pores slit and slit/cylindrical for the samples prepared in this research.

Sample	NLDFT			QSDFT		
	Fitting Error (Slit Pore) (%)	Fitting Error (Cyl. Pore) (%)	Fitting Error (Combined) (%)	Fitting Error (Slit Pore) (%)	Fitting Error (Cyl. Pore) (%)	Fitting Error (Combined) (%)
Graphite	5.296	6.819	6.819	4.364	7.510	7.510
MOF-199	0.600	0.140	0.135	0.840	0.700	0.698
SBA-15	-	0.513	-	-	-	-
GACKP	0.499	0.335	0.300	0.138	0.057	0.030
MCM-41	-	3.100	-	-	-	-

3.2. Thermogravimetric (TG) Analysis of Samples

The thermogravimetric analysis (TGA) for each of the samples was carried out in order to analyze its thermal stability. The TG and DTG of the solids under study are shown in Figure 3a,b. The TG/DTG of the MOF-199 presents two thermal events: the first observed weight loss (~9.5%) is below 200 °C and is attributed to the removal of remaining solvent and desorption of water molecules. The second weight of about ~38% occurred at ~300–380 °C, which is related to the decomposition of the organic linker group, benzentricarboxylic acid. After this temperature, the observable thermal events do not reveal significant changes, which indicates the formation of CuO, which takes place above 350 °C [68].

The TGA of the MCM-41 is also presented in Figure 3. The weight loss of 9.1% due to physisorbed water molecules, after that, the dehydroxylation of the Si-OH groups occurs continuously well above 100 °C and respective mass losses are not evidenced. On the basis of anhydrous silica, the concentration of Si-OH groups bound to hydrogen is approximately 2.1/nm^2 [69].

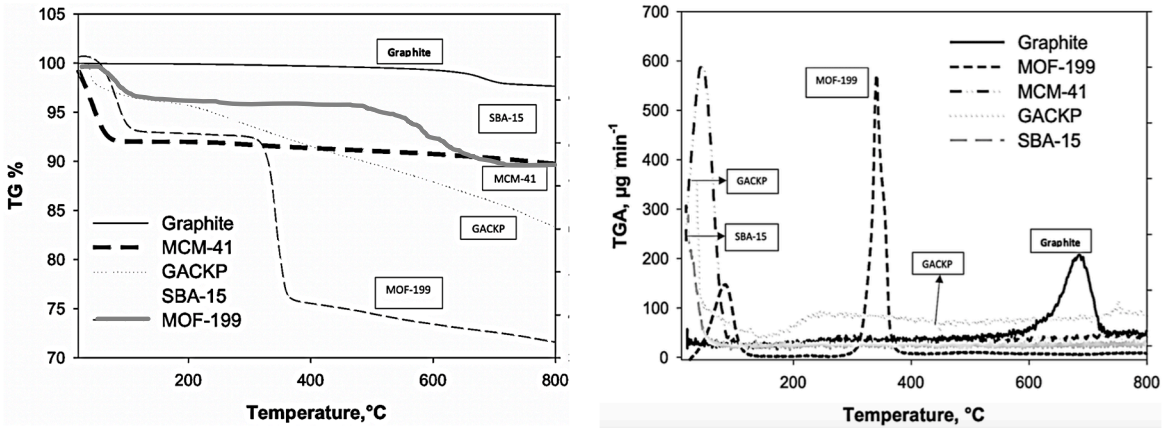

Figure 3. (**a**) TGA and (**b**) DTG of MOF-199, MCM-41, SBA-15, GACKP and Graphite.

The TGA of the SBA-15 (Figure 3) shows a weight loss below 95 °C of approximately 7%, due to the physical removal of water molecules adsorbed, while the soft weight loss presented in the range of 100–700 °C, might be associated with the decomposition of the surfactant into the pores and the condensation of silanol groups on the surface to form siloxane at higher temperatures [70].

The TGA of the GACKP is shown in Figure 3. There, a loss of mass of 4.5% below 100 °C can be observed, which indicates the humidity of the GACKP sample. Between 180 and 800 °C, a continuous mass loss (12%) is observed related to the decomposition of the solid in CO_2 and CO because the carbonaceous surfaces are normally oxidized, which is why the mass loss can be associated to the decomposition of the surface carbon-oxygen compounds. It is worth noting that the TG/DTG profiles corresponding to this sample are very clear and simple compared to other solids obtained from

lignocellulosic residues, which indicates that the combined activation with phosphoric acid and KOH allows the formation of thermally stable carbonaceous structures. The TG/DTG corresponding to the graphite can be seen in Figure 3a,b, showing that the solid begins to lose weight at approximately 570 °C, suggesting the decomposition of the surface carboxyl compounds in graphite structure at this temperature.

3.3. XRD and FTIR Analysis of Samples

The purity of the crystalline phase of MOF-199 was confirmed by XRD powder analysis. The diffraction peaks of MOF-199 were consistent with the theoretical patterns of the single crystal data and those previously reported in the literature. In addition, the XRD reflections of the CuO derived from the MOF exhibit pure phase nature without any phase of impurities such as Cu, Cu_2O and $Cu(OH)_2$ [16,71–73] (Figure 4a).

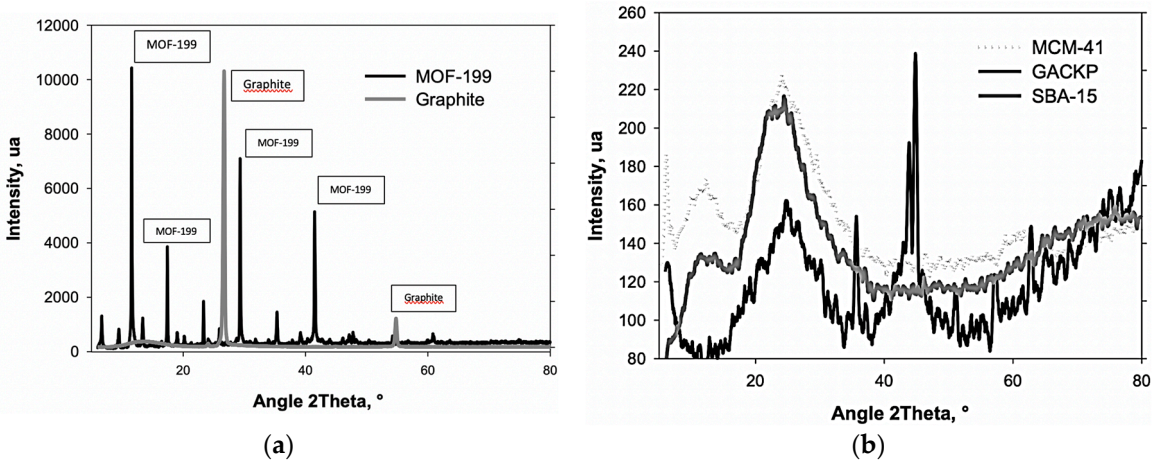

(**a**) (**b**)

Figure 4. (**a**) XRD of MOF-199 and Graphite; (**b**) XRD of MCM-41, SBA-15 and GACKP.

The observed reflections are adjusted according to a monoclinic structure with the space group C2/c. The values of the reticular structure parameters were calculated from Rietveld refinement and were found to be a = 4682 (7), b = 3427 (6), c = 5132 (2) and β = 99,322, which are consistent with the values in the literature (JCPDS Card no.48–1548). The average value of the crystallite size is also found at 21 nm according to the Scherrer equation [73].

The peaks of absorption at approximately 1650, 1565 and 1380 cm^{-1} were assigned to the vibrations characteristic of groups C=O, the peaks at approximately 1445 cm^{-1} were attributed to the stretching of C=C in the benzene ring [74] and the peaks at approximately 670 cm^{-1} are related to the stretching vibrations of Cu-O [75]. In addition, the wide peak around 3435 cm^{-1} in the FTIR spectrum of MOF-199 could be assigned to the vibration of -OH groups and coordinated or uncoordinated water molecules [76].

The XRD diffractograms (X-ray diffraction) for the sample of MCM-41, are shown in Figure 4b. Regarding the XRD of the MCM-41, the peaks attributed to this structure were also detected for the support synthesized at 2.1° and 3.5°, which correspond to the diffraction planes (1 0 0) and (2 0 0) of this material [62]. When examining the XRD at greater angles (Figure 4b), the presence of amorphous SiO2 (broad diffraction peak around 26.3°) is clearly observed.

The FTIR corresponding to the MCM-41 sample prepared for this study is shown in Figure 5a. The spectrum shows characteristic bands at 1110 and 825 cm^{-1} that can be assigned to the asymmetric and symmetric stretching vibration modes of the Si-O-Si species, respectively [77,78]. A band towards 980 cm^{-1} can be attributed to the tension of the Si-OH bonds present in the sample MCM-41.

The XRD patterns for SBA-15 are shown in Figure 4b. The sample of the SBA-15 shows a large wide peak between 2θ = 12 and 32 Å which shows that it is amorphous nature. The two reflections of

Brag corresponding to peaks (1 1 0) and (2 0 0) at the mid-range of the 2-theta angle suggest that these materials have highly ordered hexagonal mesostructures in 2-D [79].

The FTIR spectrum of the SBA-15 are presented in Figure 5a. In the spectrum, two strong absorption peaks are observed at 1100 and 820 cm^{-1} assigned to the asymmetric and symmetric vibration modes of the inorganic framework Si-O-Si [80]. The characteristic band of the Si-OH stretch mode is around 970 cm^{-1}. These bands corroborate the chemical nature of the SBA-15 and its satisfactory synthesis. Additionally, the FTIR spectrum of SBA-15 showed a wide and intense peak at 3550–3350 cm^{-1}, which was assigned to the silanol group (Si-OH) or "networks" of silanol with crossed hydrogen bonds [76].

The XRD patterns for GACKP present (Figure 4b) two broad peaks around 12° and 25° corresponding to (0 0 2) and (1 0 0) planes, respectively [66]. This type of behavior is in good agreement with other reported results for this type of solids and the amorphous nature of the sample. Figure 5b shows the FTIR spectrum of GACKP scanning from 400 to 4000 cm^{-1}. The observed O-H stretching around 3445 cm^{-1} was attributed mainly to chemisorbed water molecules and hydroxyl groups on the surface of the material. On the other hand, the stretch corresponding to C-H was observed around 2950 cm^{-1}. The bands located around 1650 cm^{-1} are assigned to the characteristic olefin group (-C = C-), which suggests that some graphitization is presented for the GACKP sample [81].

With respect to the XRD patterns of the graphite in Figure 4a, it is observed that the material is highly structured and organized. This can be verified by seeing the good definition of the peaks and the high resolution of the peak (0 0 2), at an angle of 2θ corresponding to 26.3° (KαCu). This value corresponds to an interatomic distance (d002) of 3.36 Å. Figure 5b shows the FTIR corresponding to the graphite sample used in this study. The spectrum is characteristic of a sample of this type widely reported and analyzed in the scientific literature. The approximate band at 3410 cm^{-1} is attributed to the -OH stretch vibration of hydroxyl groups and water molecules [79]. The bands centered at 1750–1710 cm^{-1} correspond to the stretching vibrations C=O of the carbonyl and carboxylic groups [36,59]. The bands located at 1620–1630 cm^{-1} resulted from the C=C stretching mode of the graphitic domains without oxidation [8]. In addition, the peaks attributed to the deformation vibration of the tertiary C-OH groups appeared at 1400 cm^{-1} [38,82]. The peaks located at approximately 1225 and 1080 cm^{-1} correspond to the stretching vibrations of C-O-C and C-O, respectively [82–85].

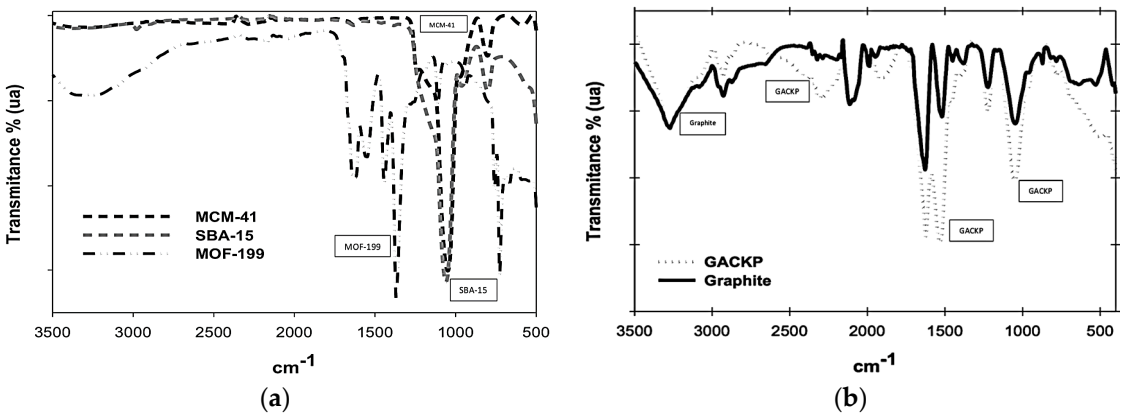

Figure 5. (**a**) FTIR spectra of MOF-199, MCM-41 and SBA-15; (**b**) FTIR spectra of GACKP and Graphite.

3.4. SEM-EDX Analysis

Figure 6(a1) shows the scanning electron microscopy (SEM) for the MOF-199 where there are some characteristics of small particles such as solids. In Figure 6(a2), as expected, the SEM micrograph for MOF-199 showed that a highly crystalline material was obtained (Figure 6a). The MOF-199 crystals in the SEM images have a double-sided pyramidal shape with a width of approximately 10–20 μm.

The SEM of sample MCM-41 is presented in Figure 6b. The morphology is similar to the material described in the literature as "wormy" MCM-41 [12]. The SEM images show slightly elongated particles

with an average width of 3.5 µm and length of 7.3 µm. It is possible to present some agglomeration forming a massive morphology with the worm texture previously mentioned [46,85]. Figure 6(b1) shows at the macroscopic level some zones that allow the characteristic structure of the MCM-41 to be seen; Figure 6(b2) shows that if the image is taken closer the structure of this solid is better shown.

The Figure 6c shows the SEM taken at the synthesized SBA-15, it has several string-like domains with uniform sizes of 1 µm, which are aggregated as wheat-like macrostructures [46,47]. In Figure 6(c1) some chains are superimposed on each other. In Figure 6(c2) these chains are clearly seen, which as mentioned, they are characteristic of SBA-15.

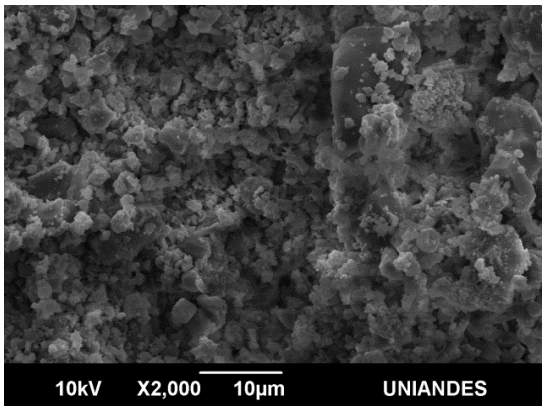

(**a1**)

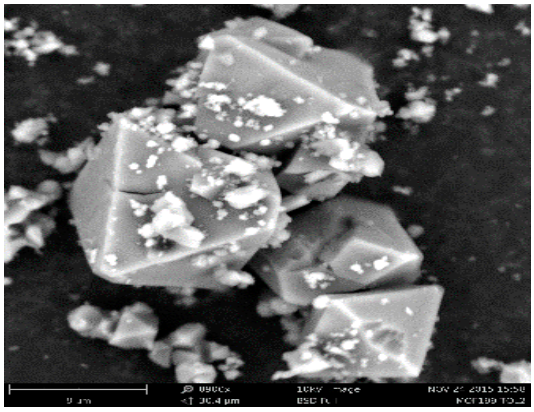

(**a2**)

(**a**) **MOF-199**

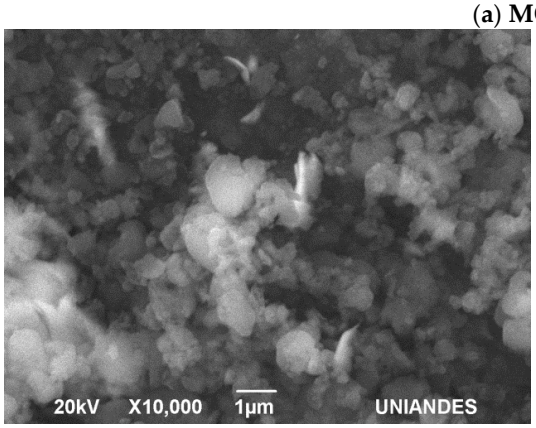

(**b1**)

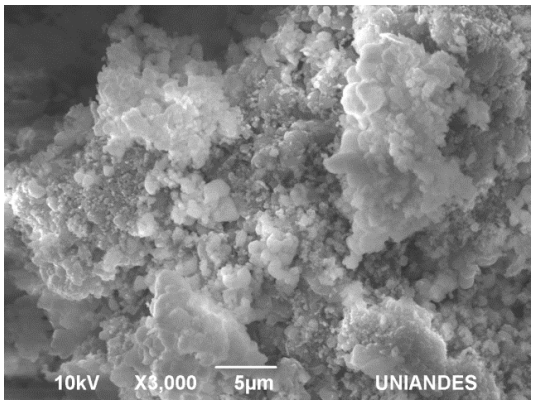

(**b2**)

(**b**) **MCM-41**

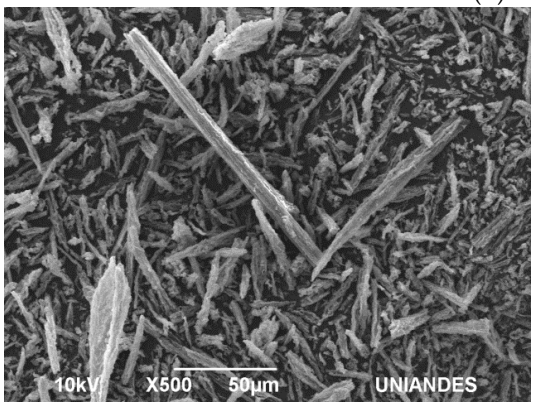

(**c1**)

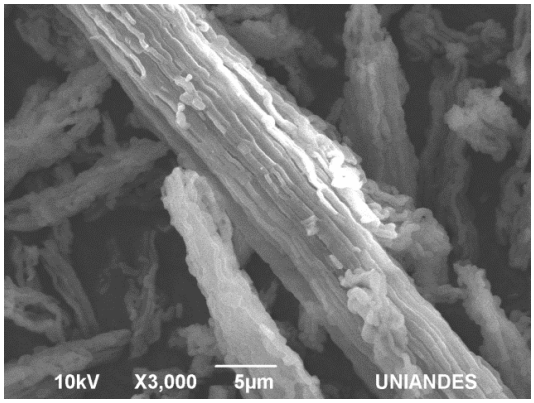

(**c2**)

(**c**) **SBA-15**

Figure 6. *Cont.*

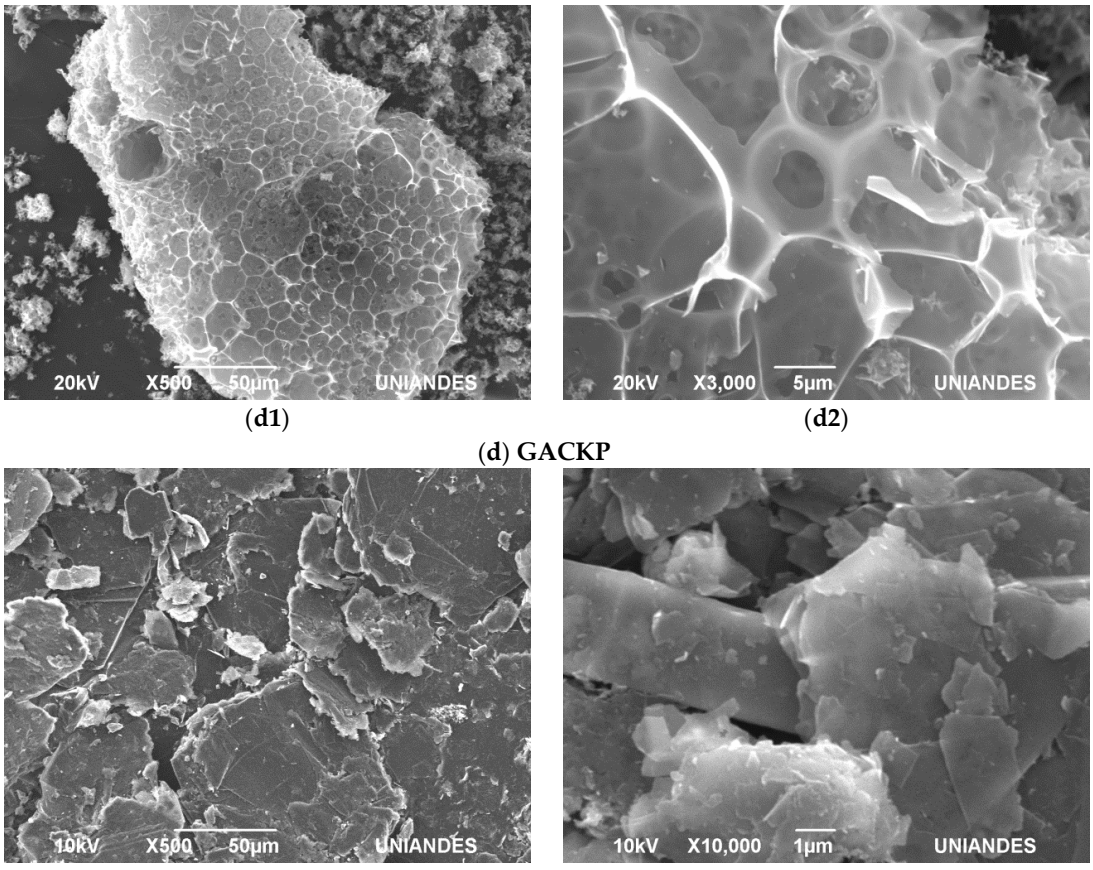

(**d1**) (**d2**)

(**d**) **GACKP**

(**e1**) (**e2**)

(**e**) Graphite

Figure 6. Scanning electron microscopy (SEM) micrographs of solids (**a**) MOF-199; (**b**) MCM-41; (**c**) SBA-15; (**d**) GACKP; (**e**) Graphite.

Figure 6d shows the SEM corresponding to the GACKP sample. The sample presents a well-developed porous structure with pores of different sizes, which allows verifying that it has heterogeneous textural properties as analyzed in the previous section. In Figure 6(d1) the characteristic porosity of an activated carbon prepared under the conditions of this investigation was clearly observed. In Figure 6(d2) (magnified), clearly developed pores were seen.

Finally, Figure 6e shows the SEM obtained for the graphite sample. It can be clearly seen that the SEM images have a certain layered structure in the form of sheets that are tightly integrated between layers and layers. In Figure 6(e1) there is a microphotograph for graphite where the layers overlap each other, similar to "book sheets." The micrograph of Figure 6(e2) shows an approximation of the previous image and presents some layers in detail.

In summary, we have characterized the five samples that were used in this investigation to perform comparative studies based on isosteric heats. As shown, the samples differ widely in their textural characteristics (area, pore volume, pore distribution, etc.) and in their chemical nature.

3.5. Isosteric Heat: Comparison of CSK, C-C and Adsorption Calorimetry (A-Cal) Methods

Figure 7a–e shows the corresponding results for the calculation of isosteric heats for each of the samples prepared in this work. Each graph presents the isosteric heat calculated by each method used in this investigation (CSK, C-C and A-Cal).

Figure 7a shows the isosteric heats of MOF-199. The figure presents curves with very similar behavior: initially, they decay from approximately a value of -48 kJ·mol^{-1} to a value of -27 kJ·mol^{-1} where later they reach a plateau. This zone is very characteristic for solids of this type and is typical of

thermal behavior of the isostere on a heterogeneous surface [22,31,33]. In this area the values evaluated by the three methods are very similar, however, with the low standard deviation of the adsorption calorimetry (A-Cal), it is observed that the indirect methods always underestimated the heat. In the area where the plateau is reached, which ranges from 1 to 3.5 mmol·g^{-1}, corresponds to isosteric heats that occur on homogeneous surfaces [22,31]. Subsequently, there is an increase in the enthalpic value of isosteric heat of −32 to −48 kJ·mol^{-1}, which is probably due to interactions of the N_2 molecule within the porous structure of MOF-199. In this zone, the values calculated by C-C and CSK are below with respect to the direct measurement method using the adsorption calorimetry methodology. As mentioned above, the low standard deviation of the adsorption calorimetry allows differentiation of the heat released in the adsorption with respect the calculated ones. The adjustment of each of the methods used to calculate the isosteric heats is dependent on the porosity of the MOF. The isosteric heat of the experiment decreases with the coverage to the condensation step.

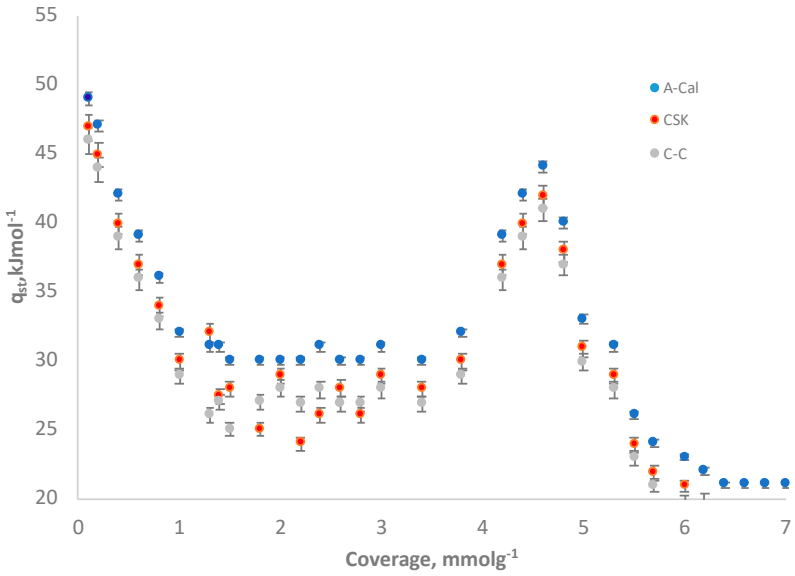

(**a**) MOF-199

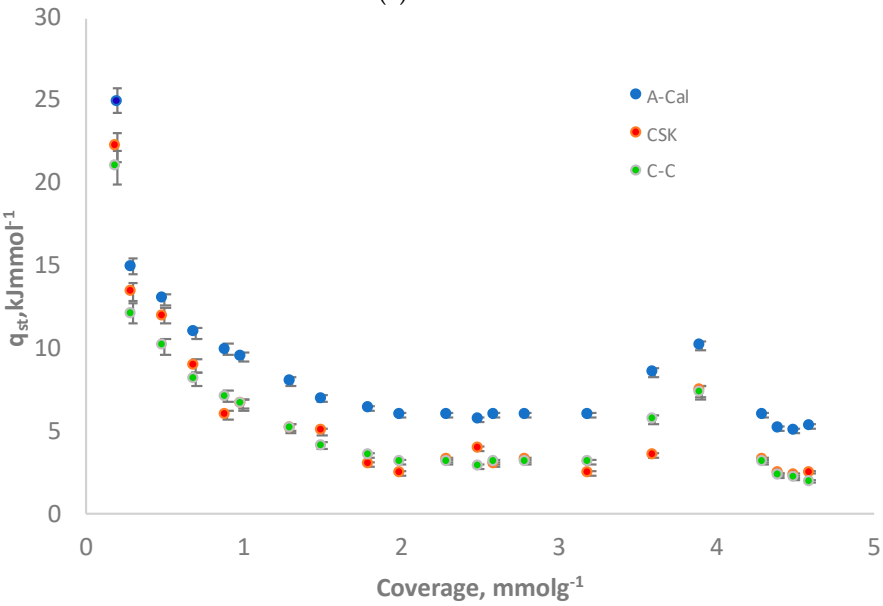

(**b**) MCM-41

Figure 7. *Cont.*

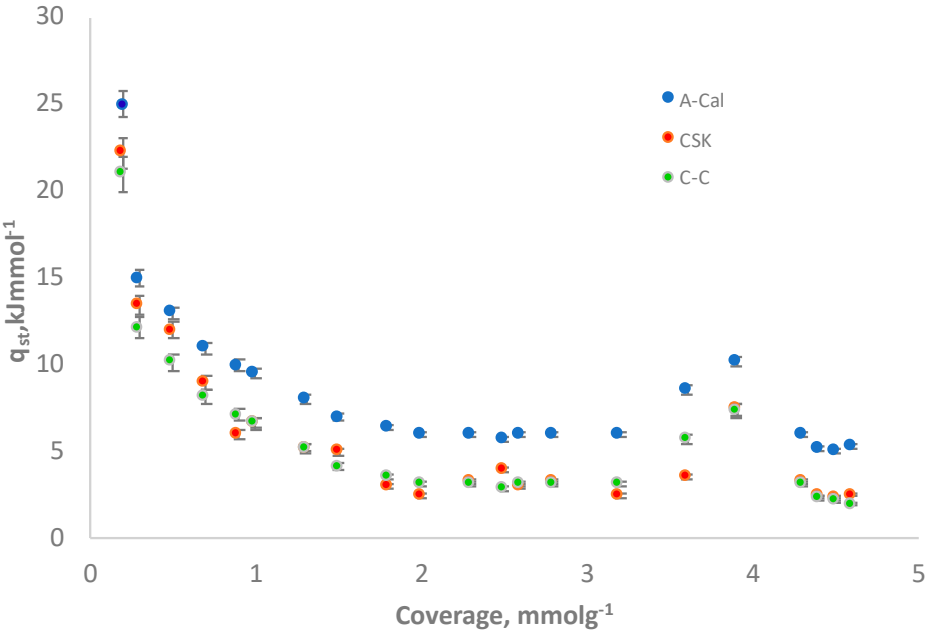

(**c**) SBA-15

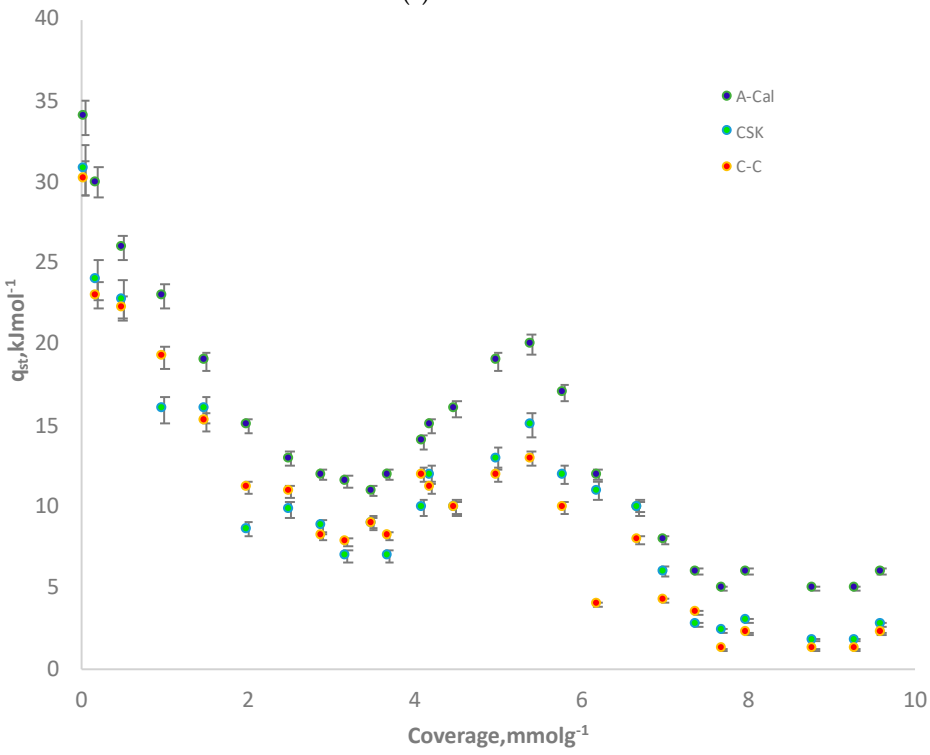

(**d**) GACKP

Figure 7. *Cont*.

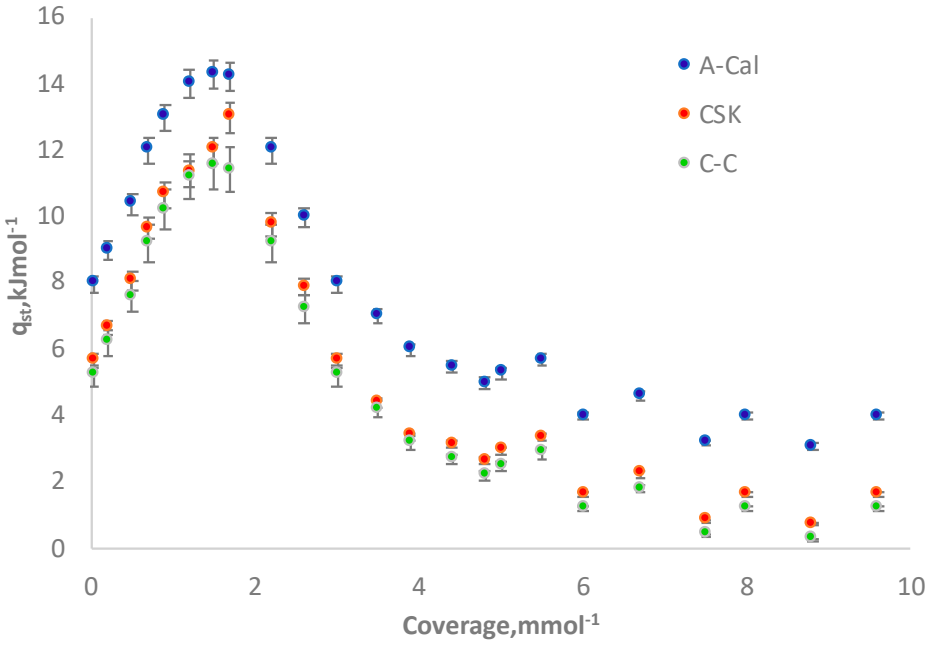

(**e**) Graphite

Figure 7. Isosteric heats of adsorption for N_2. (**a**) MOF-199; (**b**) MCM-41; (**c**) SBA-15; (**d**) GACKP; (**e**) Graphite.

The results of the isosteric heats obtained for the MCM-41 are presented in Figure 7b. In the diagrams it can be clearly seen that during the initial region where the first layer of the adsorbate is formed, the isosteric heat changes according to the method used to evaluate it, A-Cal and the CSK and C-C, and they are not coincident, because the confidence intervals for each method are significantly different (deviation bars in the figure). It is likely that the differences between the two calculation methods and the experimental one (adsorption calorimetry) can be attributed to the mechanism of N_2 adsorption on a mesostructured porous network like the MCM-41 surface. The C-C and CSK methods by their nature of the determination do not contemplate the heterogeneity of the surface. Adsorption calorimetry, because it is a direct measurement method, can be recorded because it directly measures the thermal effect generated as the coating is made with the N_2 molecules at that temperature. This zone is between 0.5–2.5 mmolg^{-1} where isosteric heat decrease to values close to -12 kJmol^{-1}. Despite this, we observed that the heats are comparable between those evaluated by the CSK and C-C methods and the A-Cal method in the multilayer zone and the condensation step. Subsequently, the isosteric heats present a slight increase that may be associated with interactions between molecules of N_2 into the pore system.

The isosteric heats corresponding to the SBA-15 sample are presented in Figure 7c. This Figure presents three well-differentiated areas, like this: the first one starts at a value of -25 kJ·mol^{-1} and falls to -2 kJ·mol^{-1}, this zone corresponds to the adsorption of N_2 molecules on the homogeneous surface of SBA-15. When comparing the results obtained by the CSK and C-C methods it is possible to observe some inconsistencies between the calculated heats. The different mechanism that involves the N_2 adsorption in silica micropores and mesopores clearly affects the modeling of the experimental data with the indirect methods, but there is a better description of the adsorption process from the values obtained directly by the adsorption calorimetry method. This demonstrates the sensitivity of the calorimetric method to directly measure such effects. The next zone corresponds to a false plane followed by a wavy section that is assigned to the interaction with a surface of homogeneous characteristics; this value is between 4.5 and 6.6 mmolg^{-1} of N_2 coverage. In this area, the experimental points tend to coincide better. However, it is clear that the adjustments of the results are subject to the textural distribution of each solid.

The results obtained for the GACKP samples are presented in Figure 7d. The figure presents three perfectly differentiated zones: the first starts from -32 kJ·mol^{-1} and falls to -13 kJ·mol^{-1} corresponding to the heterogeneous zone of the GACKP sample. Subsequently, a plateau is reached at a N_2 coverage between 2.5 to 4.5 mmol·g^{-1}, which is the energy-homogeneous zone. In the last zone, there is an increase in the values of isosteric heats that correspond to the interactions among the molecules and then falls again. In this sample, it is clearly observed that the values for the isosteric heats using the CSK, C-C and A-Cal methods do not coincide in any part of the zone.

Figure 7e shows the isosteric heats obtained for the graphite. The results obtained with the different methods of evaluation of isosteric have good agreement among them, in spite of the differences in each method used to perform the calculation and instrumentation, as it is the case of the adsorption calorimetry. At low adsorbate coverage (<0.4 mmol·g^{-1}), an increase in isosteric heat is observed with the amount adsorbed. This behavior has been assigned by several authors to the formation of a monolayer and is related to a maximum value isosteric heat [22,31]. In the specialized literature, the presence of this peak on this material has been widely analyzed [22,31,33,40]. Some authors argue that the peak is related to the presence of a two-dimensional phase of a transitory phase on the surface of graphite [30,32,40]. The transient phase is characterized by the spatial rearrangement of the N_2 molecules on the surface of the graphite from a disordered state (fluid) to a "localized" or "solid state" (crystalline state). Some authors have also proposed that the presence of the peak can be an indicator of the degree of graphitization [15]; at a lower degree of graphitization, the peak is lower. It should be noted that the results obtained by adsorption calorimetry are better adjusted and describe the presence of the peak, with the C-C method being the method that presents the results with greater dispersion. After the peak, the values of isosteric heats decline to show some wave behavior. It is necessary to emphasize that the isosteric heats of adsorption are a critical variable to estimate the performance of a process during the adsorption and separation of gas in engineering. Additionally, sorption processes of gases and vapors on the porous solids, e.g., like zeolites or activated carbons have still a considerable potential for a growing number of processes in separation technology, purification of technical gases and air processes, and also for air conditioning systems [1–5,86–89]. This is reflected not only in an increasing number of scientific and technical papers, patents, and engineering reports but also in a still growing world market for plants for air separation, hydrogen and natural gases and many more [9,88–92].

Additionally, it is necessary to accurately determine the isosteric heats of adsorption of the respective adsorbate on the adsorbent and the pressure with which these heats of isomeric adsorption are determined, so, an adequate characterization of the adsorbents can be achieved, and their possible applications can be established for science and engineering. This is reflected not only in a growing number of scientific and technical documents, patents and engineering reports but also in a constantly growing world market for plants for the separation of air, hydrogen and natural gases, the preparation of materials for medical uses and many more [6–8,88–90]. Therefore, in this study, the determination of these heats allows characterization of the adsorbent material from the energetic point of view [9–11,88,89]. These results are contributing within the area in order to help scientists to have an additional criterion; also using other adsorbate-adsorbent systems can provide basic data for the development of new theories of equilibrium and adsorption kinetics; and finally, they can design adsorption and desorption processes in engineering such as PSA, VSA, TSA and combinations thereof [1,12]. In the scientific literature, several authors have undertaken analyses where they mention that the results of measurements by different methods and calculations of isothermal heats can present errors of 10% or more, sometimes reaching more than 100%. According to our results, the isosteric heats of adsorption for the used adsorbates varied according to the performed method. Figure 7 showed that the values changed according to the solid employed, especially in terms of textural characteristics, and further if the surface is energetically homogeneous or heterogeneous, besides of the quantity of adsorbed gas. This is a very important consideration for a process where there is a gas–solid interaction. Ignoring these features in the design process can lead to serious errors, such as reported by other

authors. With the results obtained, it is shown that the adsorption calorimetry allows the establishment of values of the isosteric heats of adsorption with an error of less than 2% (the statistical study is not shown here) and also reveals the complex nature of the heterogeneity or homogeneity of the adsorbent. With the methods of C-C and CKS, results depend on the solid that is used and thus errors increase. For example, for SBA-15 and activated carbon (GACKP) whose pores are less uniform than those of other adsorbents, the experimental values for these two methods had greater dispersion. This is a plus of this investigation because it demonstrates that adsorption calorimetry is useful to determine accurate values of the isosteric heats of adsorption and additionally for establishing the type of surface that has the corresponding adsorbate.

Although, it is true that the results using the CSK equation, derived from the classic Clausius–Clapeyron (C-C) equation to evaluate isosteric heats of adsorption and from thermodynamic bases in several published works, had shown that it can predict these heats with more accuracy than the classical C-C equation because this equation incorporates the additional gradients of P and T with respect to m_a. Our results show that, in general, the equations of C-C and CSK generate results in good agreement; however, the results obtained by means of C-C are more dispersed for the adsorbents with more heterogeneous porosity distribution, which does not occur with the results using the equation proposed by CSK. However, using the CSK equation, according to the results presented in Figure 7, at low quantities of N_2 a slight dispersion of the results is obtained. In a particular way this is shown in the samples SBA-15 and GACKP. This also occurred using the C-C equation, although with greater dispersion. This can be associated with the approximations of the Clausius–Clapeyron equation and that CSK equation tries to improve C-C. It is worth remembering that Chakraborty et al. developed the model to calculate isosteric heats for low and high adsorption pressures. The significant characteristic of the Chakraborty model is the addition of the pressure gradient term for the gas phase to the Clausius–Clayperon equation [50–52,93,94]. However, as other authors proposed [23–26,53,54,93,94], in the model, the ideal gas assumption was adopted, while the volume of the adsorbed phase was neglected. Rahman et al. [53,54] proposed an isosteric heat model in which the adsorbed phase volume took into account the pressure gradient term of the Clausius–Clayperon equation. However, the perfect gas assumption was still involved, and the volume of the adsorbed phase was neglected, what was similar to Chakraborty et al. Attempts have been made to address the non-ideality of the adsorbed phase, as well as the volume of the adsorbed phase [23–26,56–59,94]. However, the latent heat was still adopted in its formulation, while the actual gas correction was achieved by using the pressure-volume ratio for the adsorbed phase and the liquid phase. Lately, the heat of adsorption was expressed in terms of fugacity of gases by Tian et al., and validated with differential heat of adsorption data from large Monte Carlo simulations (GCMC) [59,93,94]. Therefore, it is evident that the ability of thermodynamic model to accurately predict isosteric heat for the adsorption process ranging from partial vacuum to supercritical temperature is, until now, quite limited. Throughout the coverage examined in this work, the isosteric heats evaluated by adsorption calorimetry are larger than the evaluated by C-C and CSK indirect methods of vaporization, for nitrogen. This means that the molecules within the micropores are always affected by the potential field and they do not show any saturation unlike what happens when the adsorption occurs on the external surface of the material. This may be related to the experimental method of adsorption calorimetry and its sensitivity: when the molecules of nitrogen enter to a pore, these are subject to the potential of the respective pore and the pressure transducers of the calorimeter are able to record this solute–adsorbent interaction, an interaction that is not registered by the C-C and CSK methods due to the sensitivity that is required to measure this phenomenon, so that the isothermal heat values reported by these methods sub-estimate the real values. It is necessary to clarify that these results vary with the characteristics of the solids and as it has been shown in this work, by the method of measurement. This is another aspect of the novelty of this research.

4. Conclusions

A set of porous solids with different textural properties were characterized by N_2 isotherms and XRD. Among the main findings are the disorganized structure and surface heterogeneity established by the activated carbon sample, while, graphite and mesostructured silicas seem to have a homogeneous surface related to the morphology of the pores that compose them, the slits and cylinders, respectively. For MOF-199, a combined geometry described better de N_2 adsorption experimental data.

From the chemical characterization with FTIR and TG-DTG, it is possible to study the chemical nature of the samples, evidencing the different oxygen-complex surfaces and amphoteric character of the carbonaceous and siliceous surfaces. Additionally, the great hydration capacity of the MOF-199. The TG-DTG analysis was also useful to establish the appropriate degasification temperature for the calorimetry and the adsorption isotherms

The comparison of the isosteric heats obtained from every method shows a relationship of the nitrogen adsorption heats with the specific properties of each solid. It was established from the graphics obtained, that the heats that are released respond to a different interactions due to the porosity and chemical nature of the solid. It is evidenced by the different shapes and zones found, which are a function of their structure and surface homogeneity or heterogeneity as follows: The sequences of measured magnitude for the isosteric heats oscillate between ~ -48 kJmol^{-1} (MOF-199) and ~ -14 kJmol^{-1} (graphite), which correspond to physical interactions between the nitrogen molecules and the considered adsorbents.

The use of the CSK and C-C methods present acceptable coherence, particularly for the MOF-199 and MCM-41 samples. However, for the samples which possess a more heterogeneous structure (such as SBA-15, GACKP), the methods mentioned above present great dispersion in their individual results, as well as when they are compared one to the other.

In this work, the isosteric heats of nitrogen adsorption on microporous materials measured directly using adsorption calorimetry was compared with those obtained using the indirect adsorption isosteric method, according to Clausius–Clapeyron equation and the equation modified by CSK so as to establish the reliability, limitations and assumptions of the methods. In general, for all porous solids employed, we found a very good agreement between the isosteric heats measured using the adsorption calorimetry and the adsorption isosteric method throughout the range of coverage studied. Therefore, we can conclude that the use of the simpler technique, i.e., adsorption isosteric method together with simple assumptions leads to reliable results for isosteric heats. At low quantities, the isosteric heat of nitrogen adsorption decreases in the order MOF-199, GACKP, MCM-41, SBA-15 and Graphite. The order of isosteric heats is coherent with the surface characteristics of each of the solids, especially with the pore size distribution. Finally, throughout the coverage of nitrogen examined in this work, the isosteric heats evaluated by adsorption calorimetry are larger than the evaluated by C-C- and CSK indirect methods of vaporization.

Author Contributions: Conceptualization, L.G. and J.C.M.-P.; methodology, L.G., J.C.M.-P. and P.R.-E.; formal analysis, L.G. and J.C.M.-P.; investigation, L.G. and J.C.M.-P.; data curation, L.G. and J.C.M.-P.; writing—original draft preparation, L.G. and J.C.M.-P.; writing—review and editing, L.G., J.C.M.-P. and P.R.-E.; visualization, L.G., J.C.M.-P. and P.R.-E.

Funding: This research received no external funding.

Acknowledgments: The authors thank the Framework Agreement between the Universidad de los Andes and the Universidad Nacional de Colombia and the act of agreement established between the Chemistry Departments of the two universities. The authors also appreciate the grant for funding research programs for Associate Professors, Full Professors, and Emeritus Professors announced by the Faculty of Sciences of the University of the Andes, 20-12-2019-2020, 2019, according to the project "Enthalpy, free energy and adsorption energy of activated carbon interaction and solutions of emerging organic compounds".

Conflicts of Interest: The authors declare no conflict of interest.

References

1. Myers, A.L. Thermodynamics of adsorption in porous materials. *AIChE J.* **2002**, *48*, 145–160. [CrossRef]
2. Bhatia, S.K.; Myers, A.L. Optimum conditions for adsorptive storage. *Langmuir* **2006**, *22*, 1688–1700. [CrossRef]
3. Lee, S.-J.; Bae, Y.-S. Can Metal-Organic Frameworks attain new DOE targets for on-board methane storage by increasing methane heat of adsorption? *J. Phys. Chem. C* **2014**, *118*, 19833–19841. [CrossRef]
4. Amrouche, H.; Creton, B.; Siperstein, F.; Nieto-Draghi, C. Prediction of thermodynamic properties of adsorbed gases in zeolitic imidazolate frameworks. *RSC Adv.* **2012**, *2*, 6028–6035. [CrossRef]
5. Tian, Y.; Wu, J. Differential heat of adsorption and isosteres. *Langmuir* **2017**, *33*, 996–1003. [CrossRef] [PubMed]
6. Sircar, S. Basic research needs for design of adsorptive gas separation processes. *Ind. Eng. Chem. Res.* **2006**, *45*, 5435–5448. [CrossRef]
7. Vuong, T.; Monson, P.A. Monte Carlo simulation studies of heats of adsorption in heterogeneous solids. *Langmuir* **1996**, *12*, 5425–5432. [CrossRef]
8. Shen, D.; Bülow, M.; Siperstein, F.; Engelhard, M.; Myers, A.L. Comparison of experimental techniques for measuring isosteric heat of adsorption. *Adsorption* **2000**, *6*, 275–286. [CrossRef]
9. Zimmermann, W.; Keller, J.U. A new calorimeter for simultaneous measurement of isotherms and heats of adsorption. *Thermochim. Acta* **2003**, *405*, 31–41. [CrossRef]
10. Siperstein, F.; Gorte, R.J.; Myers, A.L. A new calorimeter for simultaneous measurements of loading and heats of adsorption from gaseous mixtures. *Langmuir* **1999**, *15*, 1570–1576. [CrossRef]
11. Pinto, M.L.; Pires, J.; Carvalho, A.P.; de Carvalho, M.B. On the difficulties of predicting the adsorption of volatile organic compounds at low pressures in microporous solid: The example of ethyl benzene. *J. Phys. Chem. B.* **2006**, *110*, 250–257. [CrossRef]
12. Langmuir, I. The adsorption of gases on plane surfaces of glass, mica and platinum. *J. Am. Chem. Soc.* **1918**, *40*, 1361–1403. [CrossRef]
13. Mathias, P.M.; Kumar, R.; Moyer, J.D.; Schork, J.M.; Srinivasan, S.R.; Auvil, S.R.; Talu, O. Correlation of multicomponent gas adsorption by the dual-site langmuir model. application to nitrogen/oxygen adsorption on 5A-zeolite. *Ind. Eng. Chem. Res.* **1996**, *35*, 2477–2483. [CrossRef]
14. Bimbo, N.; Ting, V.P.; Hruzewicz-Kolodziejczyk, A.; Mays, T.J. Analysis of hydrogen storage in nanoporous materials for low carbon energy applications. *Faraday Discuss.* **2011**, *151*, 59–74. [CrossRef]
15. Bimbo, N.; Sharpe, J.E.; Ting, V.P.; Noguera-Díaz, A.; Mays, T.J. Isosteric enthalpies for hydrogen adsorbed on nanoporous materials at high pressures. *Adsorption.* **2014**, *20*, 373–384. [CrossRef]
16. Whittaker, P.B.; Wang, X.; Regenauer-Lieb, K.; Chua, H.T. Predicting isosteric heats for gas adsorption. *Phys. Chem. Chem. Phys.* **2013**, *15*, 473–482. [CrossRef]
17. Czepirski, L.; Jagiello, J. Virial-type thermal equation of gas-solid adsorption. *Chem. Eng. Sci.* **1989**, *44*, 797–801. [CrossRef]
18. Chowdhury, P.; Mekala, S.; Dreisbach, F.; Gumma, S. Adsorption of CO, CO_2 and CH_4 on Cu-BTC and MIL-101 metal organic frameworks: Effect of open metal sites and adsorbate polarity. *Microporous Mesoporous Mater.* **2012**, *152*, 246–252. [CrossRef]
19. Mishra, P.; Mekala, S.; Dreisbach, F.; Mandal, B.; Gumma, S. Adsorption of CO_2, CO, CH_4 and N_2 on a zinc based metal organic framework. *Sep. Purif. Technol.* **2012**, *94*, 124–130. [CrossRef]
20. Mason, J.A.; Veenstra, M.; Long, J.R. Evaluating metal-organic frameworks for natural gas storage. *Chem. Sci.* **2014**, *5*, 32–51. [CrossRef]
21. Myers, A.L.; Monson, P.A. Adsorption in porous materials at high pressure: Theory and experiment. *Langmuir* **2002**, *18*, 10261–10273. [CrossRef]
22. Cimino, R.T.; Kowalczyk, P.; Ravikovitch, P.I.; Neimark, A.V. Determination of isosteric heat of adsorption by quenched solid density functional theory. *Langmuir* **2017**, *33*, 1769–1779. [CrossRef]
23. Askalany, A.A.; Saha, B.B. Towards an accurate estimation of the isosteric heat of adsorption – A correlation with the potential theory. *J. Colloid Interface Sci.* **2017**, *490*, 59–63. [CrossRef]
24. Chakraborty, A.; Saha, B.B.; Koyama, S. On the thermodynamic modeling of the isosteric heat of adsorption and comparison with experiments. *Appl. Phys. Lett.* **2006**, *89*, 171901. [CrossRef]

25. Chakraborty, A.; Saha, B.B.; Koyama, S.; Ng, K.C.; Srinivasan, K. Adsorption thermodynamics of silica gel-water systems. *J. Chem. Eng. Data* **2009**, *54*, 448–452. [CrossRef]
26. Chakraborty, A.; Saha, B.B.; Koyama, S. Specific heat capacity of a single component adsorbent—Adsorbate system. *Appl. Phys. Lett.* **2007**, *90*, 171902. [CrossRef]
27. Rouquerol, F.; Rouquerol, J.; Sing, K. *Adsorption by Powders and Porous Solids: Principles, Methodology and Applications*, 1st ed.; Academic Press: London, UK, 1998; pp. 86–102.
28. Beebe, R.A.; Young, D.M. Heats of adsorption of argon. *J. Phys. Chem.* **1954**, *58*, 93–96. [CrossRef]
29. Joyner, L.G.; Emmett, P.H. Differential heats of adsorption of nitrogen on carbon blacks. *J. Am. Chem. Soc.* **1948**, *70*, 2353–2359. [CrossRef]
30. Walker, P.L., Jr. *Chemistry and Physics of Carbon*; Marcel Dekker Inc.: New York, NY, USA, 1970; Volume 6, pp. 1–124.
31. Rouquerol, J.; Partyka, S.; Rouquerol, F. Calorimetric evidence for a bidimensional phase change in the monolayer of nitrogen or argon adsorbed on graphite at 77 K. *J. Chem. Soc. Faraday Trans.* **1977**, *73*, 306–314. [CrossRef]
32. Do, D.D.; Nicholson, D.; Do, H.D. On the anatomy of the adsorption heat versus loading as a function of temperature and adsorbate for a graphitic surface. *J. Colloid Interface Sci.* **2008**, *325*, 7–22. [CrossRef]
33. Grillet, Y.; Rouquerol, F.; Rouquerol, J. Two-dimensional freezing of nitrogen or argon on differently graphitized carbons. *J. Colloid Interface Sci.* **1979**, *70*, 239–244. [CrossRef]
34. Inaba, A.; Koga, Y.; Morrison, J.A. Multilayers of methane adsorbed on graphite. *J. Chem. Soc. Faraday Trans.* **1986**, *82*, 1635–1646. [CrossRef]
35. He, Y.; Seaton, N.A. Monte Carlo Simulation of the isosteric heats—Implications for the characterization of porous materials. *Stud. Surf. Sci. Catal.* **2007**, *160*, 511–518. [CrossRef]
36. Wang, Y.; Do, D.D.; Nicholson, D. Study of heat of adsorption across the capillary condensation in cylindrical pores. *Colloids Surf. A. Physicochem. Eng. Asp.* **2011**, *380*, 66–78. [CrossRef]
37. Wang, Y.; Do, D.D.; Herrera, L.F.; Nicholson, D. On the condensation/evaporation pressures and isosteric heats for argon adsorption in pores of different cross-sections. *Colloids Surf. A Physicochem. Eng. Asp.* **2013**, *420*, 96–102. [CrossRef]
38. Bergaoui, M.; Nakhli, A.; Al-Muhtaseb, S.; Khalfaoui, M. Adsorption process of n-alkanes onto BAX-1100 activated carbon: Theoretical estimation of isosteric heat of adsorption and energy distribution of heterogeneous surfaces. *J. Mol. Liq.* **2018**, *252*, 399–407. [CrossRef]
39. Pan, H.; Ritter, J.A.; Balbuena, P.B. Examination of the approximations used in determining the isosteric heat of adsorption from the clausius-clapeyron equation. *Langmuir* **1998**, *14*, 6323–6327. [CrossRef]
40. Tranchemontagne, D.J.; Hunt, J.R.; Yaghi, O.M. Room temperature synthesis of metal-organic frameworks: MOF-5, MOF-74, MOF-177, MOF-199, and IRMOF-0. *Tetrahedron* **2008**, *64*, 8553–8557. [CrossRef]
41. Britt, D.; Tranchemontagne, D.; Yaghi, O.M. Metal-organic frameworks with high capacity and selectivity for harmful gases. *Proc. Natl. Acad. Sci. USA* **2008**, *33*, 11623–11627. [CrossRef]
42. Nguyen, L.T.L.; Nguyen, T.T.; Nguyen, K.D.; Phan, N.T.S. Metal–organic framework MOF-199 as an efficient heterogeneous catalyst for the aza-Michael reaction. *Appl. Catal. A Gen.* **2012**, *425*, 44–52. [CrossRef]
43. Rowsell, J.L.C.; Yaghi, O.M. Effects of Functionalization, Catenation, and Variation of the Metal Oxide and Organic Linking Units on the Low-Pressure Hydrogen Adsorption Properties of Metal-Organic Frameworks. *J. Am. Chem. Soc.* **2006**, *128*, 1304–1315. [CrossRef]
44. George, J.; Shylesh, S.; Singh, A.P. Vanadium-containing ordered mesoporous silicas: Synthesis, characterization and catalytic activity in the hydroxylation of biphenyl. *Appl. Catal. A Gen.* **2005**, *290*, 148–158. [CrossRef]
45. Meléndez-Ortiz, H.I.; Mercado-Silva, A.; García-Cerda, L.A.; Castruita, G.; Perera-Mercado, Y.A. Hydrothermal synthesis of mesoporous silica MCM-41 using commercial sodium silicate. *J. Mex. Chem. Soc.* **2013**, *57*, 73–79. [CrossRef]
46. Zhao, D.; Feng, J.; Huo, Q.; Melosh, N.; Fredrickson, G.H.; Chmelka, B.F.; Stucky, G.D. Triblock copolymer syntheses of mesoporous silica with periodic 50 to 300 angstrom pores. *Science* **1998**, *279*, 548–552. [CrossRef]
47. Zhao, D.; Huo, Q.; Feng, J.; Chmelka, B.F.; Stucky, G.D. Nonionic triblock and star diblockcopolymer and oligomeric surfactant syntheses of highly ordered, hydrothermally stable, mesoporous silica structures. *J. Am. Chem. Soc.* **1998**, *120*, 6024–6036. [CrossRef]

48. Garcia-Cuello, V.S.; Giraldo, L.; Moreno-Piraján, J.C. Synthesis, Characterization, and Application in the CO Oxidation over a Copper Nanocatalyst Confined in SBA-15. *J. Chem. Eng. Data.* **2011**, *56*, 1167–1173. [CrossRef]
49. Fonseca-Correa, R.A.; Giraldo, L.; Moreno-Piraján, J.C. Trivalent chromium removal from aqueous solution with physically and chemically modified corncob waste. *J. Anal. Appl. Pyrolysis* **2013**, *101*, 132–141. [CrossRef]
50. Giraldo, L.; Rodríguez-Estupiñán, P.; Moreno-Piraján, J.C. A microcalorimetric study of methane adsorption on activated carbons obtained from mangosteen peel at different conditions. *J. Therm. Anal. Calorim.* **2017**, *132*, 525–541. [CrossRef]
51. Garcia-Cuello, V.; Moreno-Piraján, J.C.; Giraldo, L.; Sapag, K.; Zgrablich, G. A new microcalorimeter of adsorption for the determination of differential enthalpies. *Micro Mesoporous Mat.* **2009**, *120*, 239–245. [CrossRef]
52. Giraldo, L.; Bastidas-Barranco, M.; Moreno-Piraján, J.C. Adsorption calorimetry: Energetic characterisation of the surface of mesoporous silicas and their adsorption capacity of non-linear chain alcohols. *Colloids Surf. A Physicochem. Eng. Asp.* **2016**, *496*, 100–113. [CrossRef]
53. Thommes, M.; Cychosz, K.A. Physical adsorption characterization of nanoporous materials: Progress and challenges. *Adsorption* **2014**, *20*, 233–250. [CrossRef]
54. Llewellyn, P.; Rodriguez-Reinoso, F.; Rouquerol, J.; Seaton, N. *Characterization of Porous Solids VII*; Elsevier: Amsterdam, The Netherlands, 2005; Volume 160, pp. 89–112.
55. Rodríguez-Reinoso, F.; Garrido, J.; Martín-Martínez, J.; Molina-Sabio, M.; Torregrosa, R. The combined use of different approaches in the characterization of microporous carbons. *Carbon* **1989**, *27*, 23–32. [CrossRef]
56. Llewellyn, P. *Recent Advances in Gas Separation by Microporous Ceramic Membranes*, 1st ed.; Elsevier: Amsterdam, The Netherlands, 2000.
57. Brunauer, S.; Emmet, P.H.; Teller, E. Adsorption of gases in multimolecular layers. *J. Am. Chem. Soc.* **1938**, *60*, 309–319. [CrossRef]
58. Dubinin, M.M. Fundamentals of the theory of adsorption in micropores of carbon adsorbents e characteristics of their adsorption properties and microporous structures. *Carbon* **1989**, *27*, 457–467. [CrossRef]
59. Gregg, S.J.; Sing, K.S.W. *Adsorption, Surface Area and Porosity*, 2nd ed.; Academic Press: London, UK, 1982; pp. 62–89.
60. Tarazona, P. Solid-fluid transition and interfaces with density functional approaches. *Surf Sci.* **1995**, *331*, 989–994. [CrossRef]
61. Leofanti, G.; Padovan, M.; Tozzola, G.; Venturelli, B. Surface area and pore texture of catalysts. *Catal. Today* **1998**, *41*, 207–219. [CrossRef]
62. Stoeckli, F.; Slasli, A.; Hugi-Cleary, D.; Guillot, A. The characterization of microporosity in carbons with molecular sieve effects. *Microporous Mesoporous Mater.* **2002**, *51*, 197–202. [CrossRef]
63. Matthias, T.; Katsumi, K.; Neimark, A.V.; Olivier, J.P.; Rodriguez-Reinoso, F.; Rouquerol, J.; Sing, K.S.W. Physisorption of gases, with special reference to the evaluation of surface area and pore size distribution (IUPAC Technical Report). *Pure Appl. Chem.* **2015**, *87*, 1051–1069. [CrossRef]
64. Zhang, Y.B.; Zhang, W.X.; Feng, F.Y.; Zhang, J.P.; Chen, X.M. A highly connected porous coordination polymer with unusual channel structure and sorption properties. *Angew. Chem. Int. Ed. Engl.* **2009**, *48*, 5287–5290. [CrossRef]
65. Lin, X.; Telepeni, I.; Blake, A.J.; Dailly, A.; Brown, C.M.; Simmons, J.M.; Zoppi, M.; Walker, G.S.; Thomas, K.M.; Mays, T.J.; et al. High capacity hydrogen adsorption in Cu(II) tetracarboxylate framework materials: The role of pore size, ligand functionalization, and exposed metal sites. *J. Am. Chem. Soc.* **2009**, *131*, 2159–2171. [CrossRef]
66. Alsmail, N.H.; Suyetin, M.; Yan, Y.; Cabot, R.; Krap, C.P.; Lü, J.; Easun, T.L.; Bichoutskaia, E.; Lewis, W.; Blake, A.J.; et al. Analysis of high and selective uptake of CO_2 in an oxamide containing $\{Cu_2(OOCR)_4\}$-based metal–organic framework. *Chem. Eur. J.* **2014**, *20*, 7317–7324. [CrossRef]
67. Banerjeea, A.; Singha, U.; Aravindan, V.; Srinivasan, M.; Ogale, S. Synthesis of CuO nanostructures from Cu-based metal organic framework (MOF-199) for application as anode for Li-ion batteries. *Nano Energy* **2013**, *2*, 1158–1163. [CrossRef]
68. Schlichte, K.; Kratzke, T.; Kaskel, S. Micropor. Improved synthesis, thermal stability and catalytic properties of the metal-organic framework compound $Cu_3(BTC)_2$. *Micro Mesporous Mater.* **2004**, *73*, 81–88. [CrossRef]

69. Zhao, X.S.; Lu, G.Q.; Whittaker, A.K.; Millar, G.J.; Zhu, H.Y. Comprehensive Study of Surface Chemistry of MCM-41 Using 29Si CP/MAS NMR, FTIR, Pyridine-TPD, and TGA. *J. Phys. Chem. B.* **1997**, *101*, 6525–6531. [CrossRef]
70. Taguchi, A.; Schüth, F. Ordered mesoporous materials in catalysis. *Micro Mesporous Mater.* **2005**, *77*, 1–45. [CrossRef]
71. Marx, S.; Kleist, W.; Baiker, A. Synthesis, structural properties, and catalytic behavior of Cu-BTC and mixed-linker Cu-BTC-PyDC in the oxidation of benzene derivatives. *J. Catal.* **2011**, *281*, 76–87. [CrossRef]
72. Xu, G.; Nie, P.; Dou, H.; Ding, B.; Li, L.; Zhang, X. Exploring metal organic frameworks for energy storage in batteries and supercapacitors. *Mater. Today* **2017**, *20*, 191–209. [CrossRef]
73. Wang, F.; Guo, H.; Chai, Y.; Li, Y.; Liu, C. The controlled regulation of morphology and size of HKUST-1 by "coordination modulation method". *Microporous Mesoporous Mater.* **2013**, *173*, 181–188. [CrossRef]
74. Nakamoto, K.; Martell, A.E. Infrared spectra of metal-chelate compounds. I. A normal coordinate treatment on Bis-(Acetylacetonato)-Cu (II). *J. Chem. Phys.* **1960**, *32*, 588–597. [CrossRef]
75. Myers, A.L.; Valenzuela, D.P. *Adsorption Equilibrium Data Handbook*; Prentice Hall: Englewood Cliffs, NJ, USA, 1989.
76. Ahemd Saidd, A.A.; Abd El-Wahab, M.M.M.; Alian, A.M. Catalytic performance of Brønsted acid sites during esterification of acetic acid with ethyl alcohol over phosphotungestic acid supported on silica. *J. Chem. Tech. Biotechnol.* **2007**, *82*, 513–523. [CrossRef]
77. Lombardo, M.V.; Videla, M.; Calvo, A.; Requejo, F.G.; Soler-Illia, G.J.A.A. Amino-propyl-modified mesoporous silica SBA-15 as recovery agents of Cu (II)-sulfate solutions: Adsorption efficiency, functional stability and reusability aspects. *J. Hazard. Mater.* **2012**, *223*, 53–62. [CrossRef]
78. Li, C.; Yang, J.; Wang, P.; Liu, J.; Yang, Q. An efficient solid acid catalyst: Poly-p-styrenesulfonic acid supported on SBA-15 via surface-initiated ATRP. *Microporous Mesoporous Mater.* **2009**, *123*, 228–233. [CrossRef]
79. Chen, L.; Hu, J.; Qi, Z.; Fang, Y.; Richards, R. Gold nanoparticles intercalated into the walls of mesoporous silica as a versatile redox catalyst. *Ind. Eng. Chem. Res.* **2011**, *50*, 13642–13649. [CrossRef]
80. Karnan, M.; Subramania, K.; Srividhya, P.K.; Sathish, M. Electrochemical Studies on Corncob Derived Activated Porous Carbon for Supercapacitors Application in Aqueous and Non-aqueous Electrolytes. *Electrochim. Acta* **2017**, *228*, 586–596. [CrossRef]
81. Chen, W.-F.; Yan, L.-F.; Bangal, P.R. Preparation of graphene by the rapid and mild thermal reduction of graphene oxide induced by microwaves. *Carbon* **2010**, *48*, 1146–1152. [CrossRef]
82. Nethravathi, C.; Rajamathi, M. Chemically modified graphene sheets produced by the solvothermal reduction of colloidal dispersions of graphite oxide. *Carbon* **2008**, *46*, 1994–1998. [CrossRef]
83. Xu, Y.-X.; Bai, H.; Lu, G.-W.; Li, C.; Shi, G.-Q. Flexible graphene films via the filtration of water-Soluble noncovalent functionalized graphene sheets. *J. Am. Chem. Soc.* **2008**, *130*, 5856–5857. [CrossRef]
84. Jiaoa, X.; Zhang, L.; Qiua, Y.; Guan, J. Comparison of the adsorption of cationic blue onto graphene oxides prepared from natural graphites with different graphitization degrees. *Colloids Surf. A Physicochem. Eng. Asp.* **2017**, *529*, 292–301. [CrossRef]
85. Gaydhankar, T.R.; Samuel, V.; Joshi, P.N. Hydrothermal synthesis of MCM-41 using differently manufactured amorphous dioxosilicon sources. *Mater. Lett.* **2005**, *60*, 957–961. [CrossRef]
86. Guthrie, C.P.; Reardon, E.J. Metastability of MCM-41 and Al-MCM-41. *J. Phys. Chem. A* **2008**, *112*, 3386–3390. [CrossRef]
87. Wongkoblap, A.; Do, D.D.; Nicholson, D. Explanation of the unusual peak of calorimetric heat in the adsorption of nitrogen, argon and methane on graphitized thermal carbon black. *Phys. Chem. Chem. Phys.* **2008**, *10*, 1106–1113. [CrossRef]
88. Sircar, S.; Mohr, R.; Ristic, C.; Rao, M.B. Isosteric heat of adsorption: Theory and experiment. *J. Phys. Chem. B* **1999**, *103*, 6539–6546. [CrossRef]
89. Ray, M.S. Adsorptive and membrane-type separations: A bibliographical update 2000. *Adsorp. Sci. Technol.* **2001**, *19*, 821–849. [CrossRef]
90. Groszek, A.J. *Adsorption and Its Applications in Industry and Environmental Protection*, 1st ed.; Elsevier: Amsterdam, The Netherlands, 1998; Volume 1–2.
91. Kast, W. *Adsorption aus der Gasphase. Ingenieurwissen-Schaftliche Grundlagen und Technische Verfahren*; Verlag Chemie: Weinheim, Germany, 1988.

92. Moreno-Piraján, J.C.; Giraldo, L. Setups for simultaneous measurement of isotherms and adsorption heats. *Rev. Sci. Instrum.* **2005**, *76*, 103–115. [CrossRef]
93. Fatin, H.M.; Azahara, S.M.; Akihiro, Y.; Akira, H.; Bidyut, B.; Sahad, K.T. Improved model for the isosteric heat of adsorption and impacts on the T performance of heat pump cycles. *Appl. Therm. Eng.* **2008**, *143*, 688–700. [CrossRef]
94. Rahman, K.A. Experimental and Theoretical Studies on Adsorbed Natural Gas Storage System Using Activated Carbons. Ph.D. Thesis, National University of Singapore, Singapore, 2011.

© 2019 by the authors. Licensee MDPI, Basel, Switzerland. This article is an open access article distributed under the terms and conditions of the Creative Commons Attribution (CC BY) license (http://creativecommons.org/licenses/by/4.0/).